Degradation of the solar cell dye sensitizer N719
Preliminary building of dye-sensitized solar cell

Vo Anh Quan
Master Thesis, 2006

Supervisor
Torben Lund
Ho Thi Cam Hoai

Department of Life Sciences and Chemistry
Roskilde University

Acknowledgements

I wish to thank to The Danish Ministry of Foreign Affairs/DANIDA that has supported the money for my five-month studying in Denmark, the peaceful and picturesque country. Beside knowledge, I have learnt a lot about lifestyles from here.

I would like to give my special thanks to my thesis supervisor, Associate Professor Torben Lund for his enthusiastic guidance to help me to accomplish my thesis.

I would also like to thank my co-supervisor Dr. Ho Thi Cam Hoai for her navigation in my thesis.

I am grateful to PhD student Rikke Degn for her guidance to me in beginning degradation experiments and building the solar cell.

I wish to thank to PhD student Nguyen Thai Hoang for his instructions to me in performing experiments and analyzing the results.

I would like to acknowledge to Peter and Jacob who help me a lot about HPLC-UV-MS system and chemicals.

I wish to express my thanks to Mr. Nader Payami, technician in University of Copenhagen who helps me in taking SEM and giving SEM-technique documents to me.

My appreciation extends to my Vietnamese friends in Roskilde University for help me to get over difficulties in my work and my life in Denmark.

Finally, I would like to express my whole-hearted gratitude to my family, my teachers, my friends and especially my girl friend in Vietnam for their love to me. It was their love that gave me the power to overcome all difficulties in the first time I stayed abroad.

Roskilde, June 2006

Table of contents

Introduction to solar energy conversion

At present, human world energy consumption is made up of about 88% fossil fuels (gas, coal and oil), 6% hydroelectricity, 6% nuclear power and tiny fraction from biomass and other solar energy sources [1]. Fossil fuels are causing environment pollution and becoming gradually exhausted. Nuclear energy obtained from nuclear fission is inquisitively dangerous and limited due to deficiency of heavy elements. Similarly, nuclear fusion has shortcomings in controlling the reaction and the formation energy. Therefore, seeking a renewable energy source has become a fashionable work. Solar energy presents as one of the best candidates.

The amount of solar energy from the sun to the earth is gigantic, i.e. $3x10^{24}$ J per year, about 10^4 times more than what mankind consumes currently. Solar energy emitted by the sun and reaching the earth's surface is a form of electromagnetic radiation that is available over a wide spectral range (300-2100 nm). In order to be used, the radiation needs to be converted into an energy form suitable for our needs. Four different types of solar energy conversion methods are currently available for this purpose. **Thermal solar energy conversion** involves the use of solar radiation to directly heat water in domestic usage. **Themoelectric solar energy conversion** involves the use of solar energy to heat water to generate steam required to rotate electricity producing turbines in power plants. **Photoelectric solar energy conversion** changes directly solar energy into electricity by solar cells. **Chemical solar energy conversion** represents the conversion of solar energy into chemical energy.

1. **Chemical solar energy conversion**

The photochemical reaction of this kind attracting much interest is photocatalytic splitting of water into hydrogen and oxygen. The advantage of hydrogen is that it can be used both as a temporary energy storage medium and as a fuel. In principle, hydrogen can be produced in almost unlimited amount from the sole feedstock: water. Water is transparent to visible light, therefore it cannot be decomposed directly but only by radiation with wavelengths shorter than 190 nm. For electrochemical decomposition of water, a potential difference of more than 1.23V is necessary between anodic and cathodic electrodes. This potential difference is equivalent to the energy of radiation with a wavelength of approximately 1000 nm, thus the visible light is used effectively in a electrochemical system to decompose water. In 1972, Fujishima and Honda invented a water photo-splitting cell based on single-crystal TiO_2 which can decompose water with visible light [2, 3]. The structure and operational principle was shown in fig. 1.

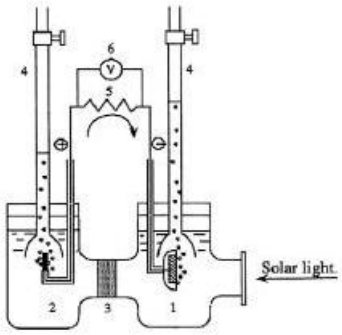

Fig. 1. Schematic diagram of an electrochemical photocell. (1) TiO_2 electrode; (2) Pt counter electrode; (3) ionically conducting separator; (4) gas buret; (5) load resistance and (6) volt-meter.

When the surface of TiO_2 electrode was irradiated with light ($\lambda < 415$ nm), electrons and holes were produced. Holes oxidized water at TiO2 electrode to produce O_2 and H^+. H^+ and electrons transported from TiO_2 to Pt electrode, then coupled to produce H_2 at Pt electrode. The reactions were presented as following equations.

$$TiO_2 + 2\,h\nu \rightarrow 2\,e^- + 2\,h^+ \quad (1)$$

$$H_2O + 2\,h^+ \rightarrow (1/2)\,O_2 + 2\,H^+ \text{ (at } TiO_2 \text{ electrode)} \quad (2)$$

$$2\,H+ + 2\,e^- \rightarrow H_2 \text{ (at Pt electrode)} \quad (3)$$

The overall reaction is:

$$H_2O + 2\,h\nu \rightarrow (1/2)\,O_2 + H_2 \qquad (4)$$

There are some problems in splitting of water using semiconductor photocatalysts. The problems lie in low efficiency, back reactions which decelerate the net reactions, and the difficulty in utilizing visible light. One solution is combination of two semiconductor electrodes: one for hydrogen evolution and the other for oxygen evolution. Fig. 2 showed the combination system based on TiO_2 particles.

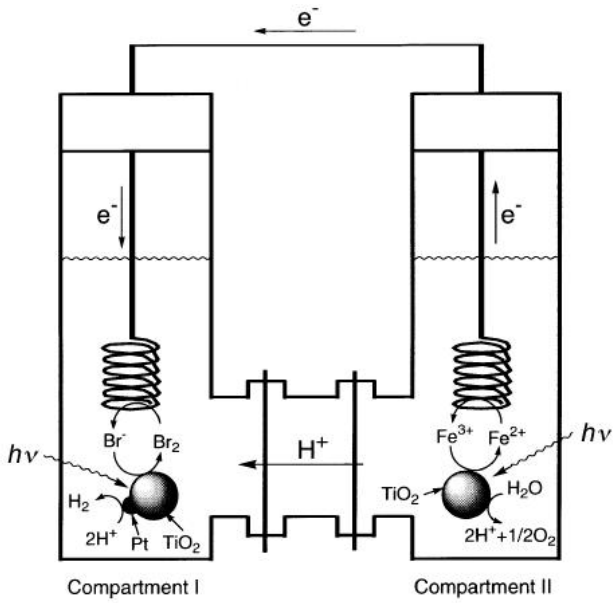

Fig. 2. Schematics of the photocatalytic cell for splitting water.

At compartment II, Fe^{3+} was used as electron acceptor and Br^- is a electron donor to help hydrogen evolution on Pt-loaded TiO_2 particles in compartment I [4].

Due to the large bandgap of TiO_2 (3.0 eV), the photocatalysis appears when irradiated with the short-wavelength light (UV). Some ways have done to obtain efficiency at longer wavelength such as coated by WO_3 [5], doped with ruthenium [6]. $TiO_{2-x}C_x$ (x = 0.15) was synthesized by flame pyrolysis of Ti metal sheet in the presence of combustion products (CO_2 and steam H_2O). This material has low bandgap energy (2.32 eV) that can absorb light with wavelength at 525 nm [7].

The other way of splitting water to H_2 is mimicking the photosynthesis in nature called artificial photosynthesis. The first part is designing of artificial photosystem II (PS II) in which visible light induces water oxidation to evolve O_2. The reaction center of photosystem II provides electrons to reduce CO_2 or reduce H^+. The overall reaction in photosystem II is shown as equation (5)

$$2H_2O \xrightarrow{\text{Molecular catalyst}} O_2 + 4H^+ + 4e^- \quad (5)$$

Many efforts have done to investigate the mechanisms of water oxidation in photosystem II. By light absorption of chlorophyll aggregate P_{680} in PS II, electron transfer occurs from the excited P_{680} to a primary electron acceptor pheophytin and subsequently to two quinines, forming P_{680}^+ radical cation. The oxygen-evolving center (OEC) in PS II serves as an electron donor to P_{680}^+, and this electron transfer is mediated by a Tyr_z residue (Scheme 1) [8].

Scheme 1. Electron transfer in PS II.

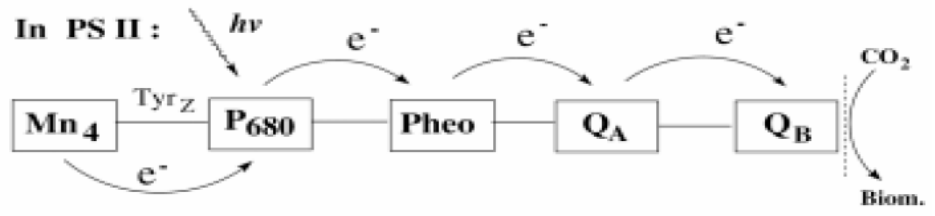

The OEC contains a unique oxo-bridge manganese aggregate responsible for the catalytic water oxidation to evolve O_2. The current model of OEC involves five intermediate states from S_0 to S_4 (Scheme 2, the so-called Kok cycle) [9].

Scheme 2. Kok cycle in OEC.

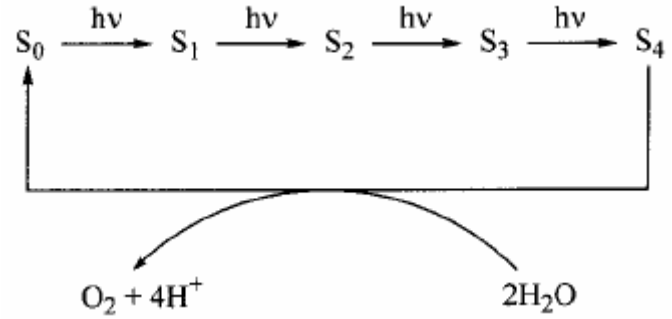

Cl^- and Ca^{2+} ions play important roles in this cycle. Many models have been proposed to this cycle. One of them is shown in fig. 3.

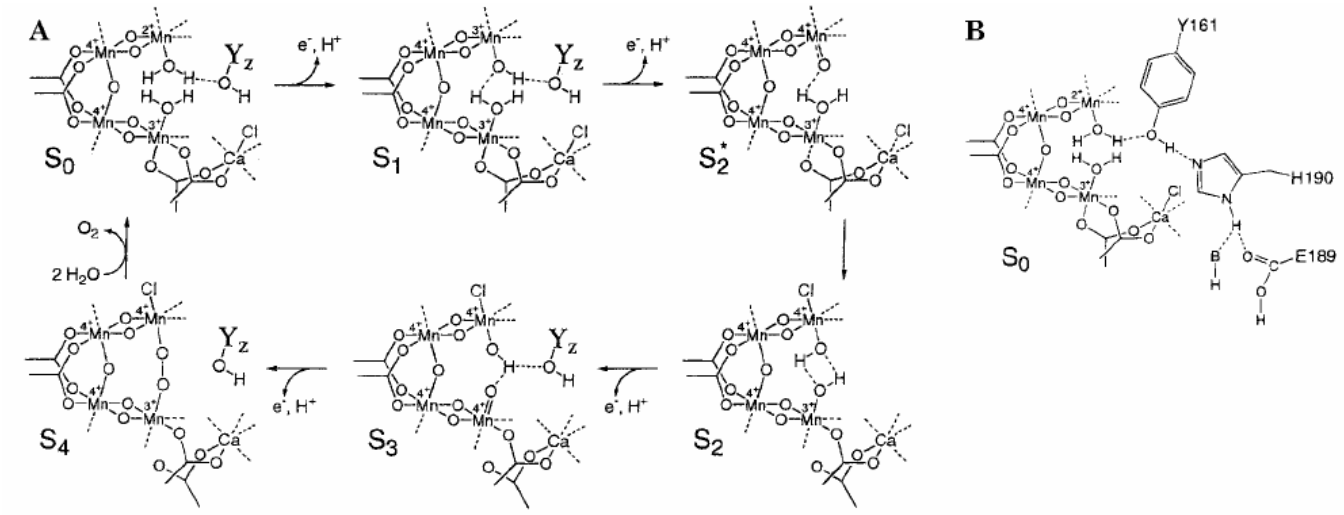

Fig. 3. Babcock's model of S state cycle (A) and the S_o state (B)

Many artificial PS II models have been proposed for water oxidation, but no efficient model has been established so far. The early artificial PS II model is based on Ru dimer $[(bpy)_2(H_2O)RuORu(H_2O)(bpy)_2]^{4+}$ and Mn-oxo cluster $(tpy)(H_2O)Mn^{III}$(di-μ-oxo)$Mn^{IV}(H_2O)(tpy)$ [10], followed by Ru-Mn complexes, Ru-Tyrosine and Ru-$(Mn)_n$ complexes via Tyrosine (fig.4). Electron acceptors used are methyl viologen or $[Co(NH_3)_5Cl]^{2+}$ [8, 11].

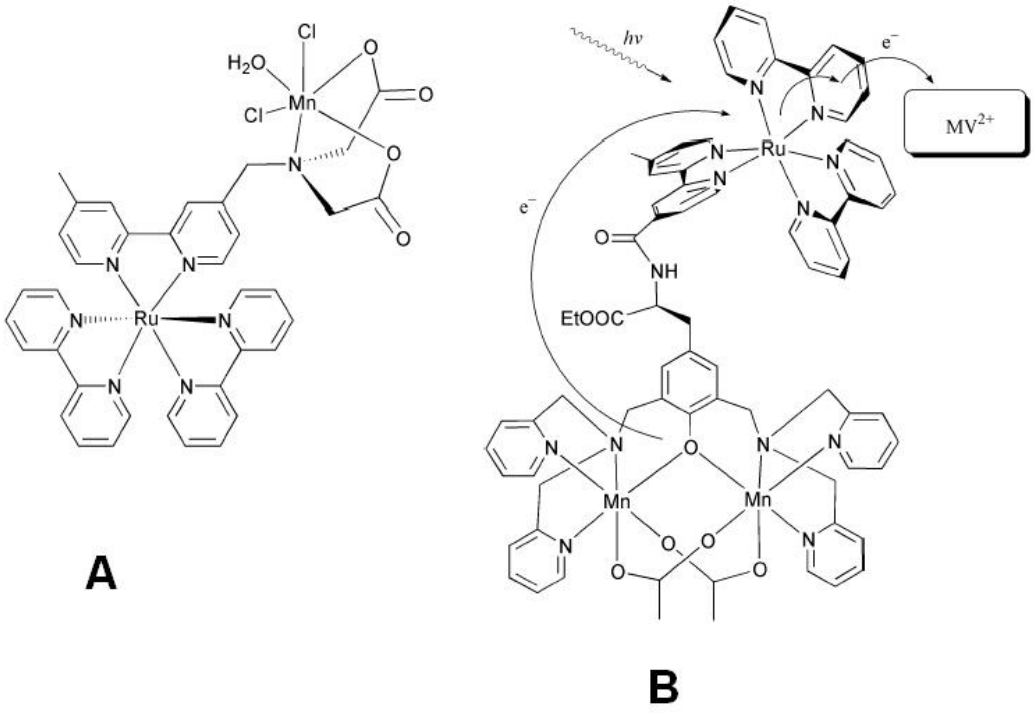

Fig. 4. Structures of Ru-Mn complex (A) and Ru-$(Mn)_2$ complexes via Tyrosine (B)

2. Solar cells

2.1 Solid state solar cells

Photovoltaic effects were firstly observed more than 150 years ago. In 1839, Becquerel detected a photovoltage when sunlight was allowed to shine on one of two electrodes placed in an electrolyte solution. In 1954, researchers at the Bell Telephone Laboratories demonstrated the first practical conversion of solar radiation into electricity via use of a p-n junction type solar cell with 6% efficiency. It was used in space program such as satellites. In the early 1970s, oil crisis led to serious consideration of photovoltaics. This work focused on improving performance, lowering costs and increasing reliability. Although photovoltaic cells come in many forms, the most common structure is based on the use of semiconductor material into which a p-n junction has been formed. Fig. 5 shows the structure of this kind of solar cells based on thin-film crystalline silicon [12].

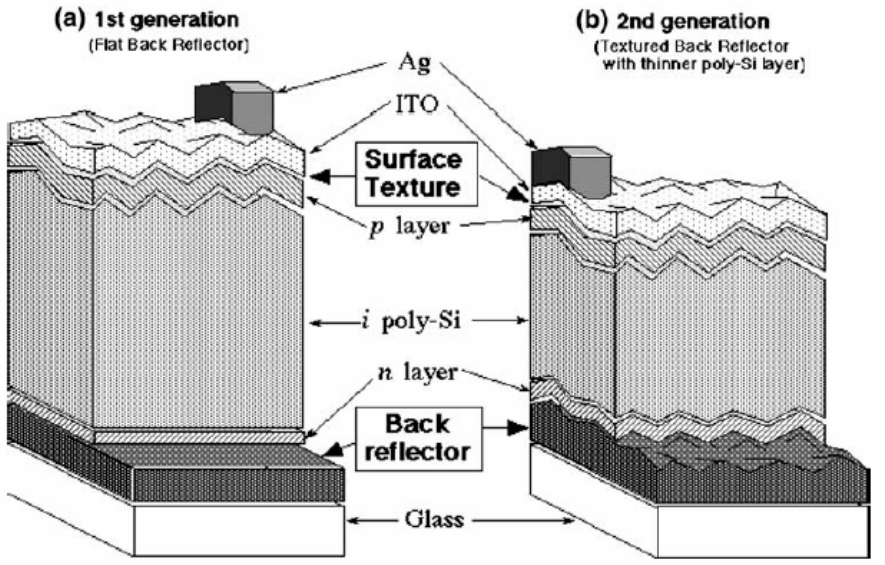

Fig. 5. Structures of silicon solar cells, the first generation a) and the second generation b).

Illumination of a p-n junction cells generates a electron-hole pair. The electron will be drawn to the n-side and the hole to the p-side to produce electric current. The electron and hole can recombine by radiative, Auger or defect level recombination. The silicon cell requires high-crystalline silicon, this causes the high price of this cell. The maximum theoretical efficiency is 33%, the best laboratory cells to be about 24%, commercial single-

crystal Si solar cell have efficiency in 12-16% range. Recently, M. Green et al. in University of New South Wales (Australia) have developed PERL cell with efficiency 24.7% (fig. 6) [13]. Many efforts in investigating this kind of cell based on low-cost amorphous silicon and the efficiency is 6-8% up to now. Other type of cells based on nearly ideal material for thin-film photovoltaics, CdTe semiconductor. The efficiency of CdTe solar cell is now 16% [14].

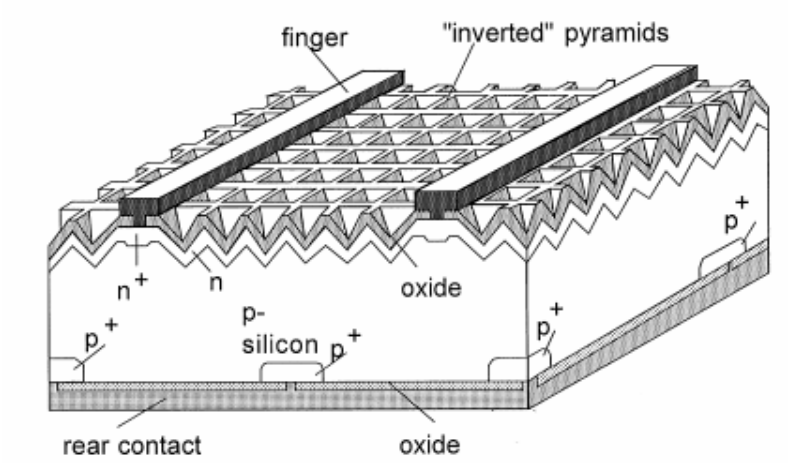

Fig. 6. PERL cell (passivated emitter, rear locally diffused)

2.2 Organic solar cells

Organic materials as, e.g. conjugated polymers, dyes or molecular organic glasses can show p-type or n-type semiconducting properties. Extremely high optical absorption coefficients are possible with these materials, which offer the possibility for production of very thin solar cell and therefore only very small amount of needed materials. The variability of organic compound is nearly infinite. Beside this, from the technological aspects, these materials show the ease of large-scale manufacturing at low temperature and very low costs. The typical bi-layer cell was shown in fig 7. Some of materials for organic solar cell were presented in fig. 8 [15].

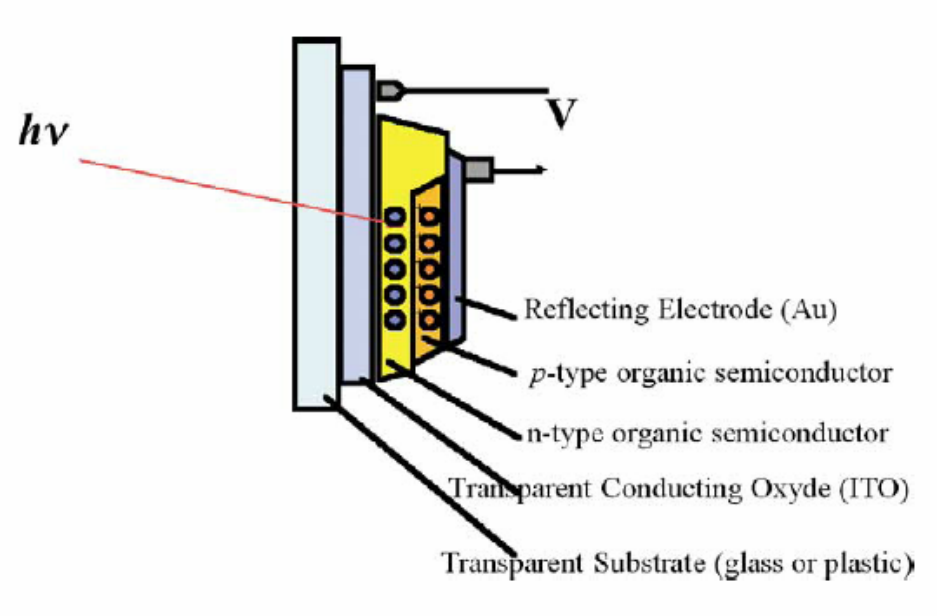

Fig. 7. Typical bi-layer organic solar cell design.

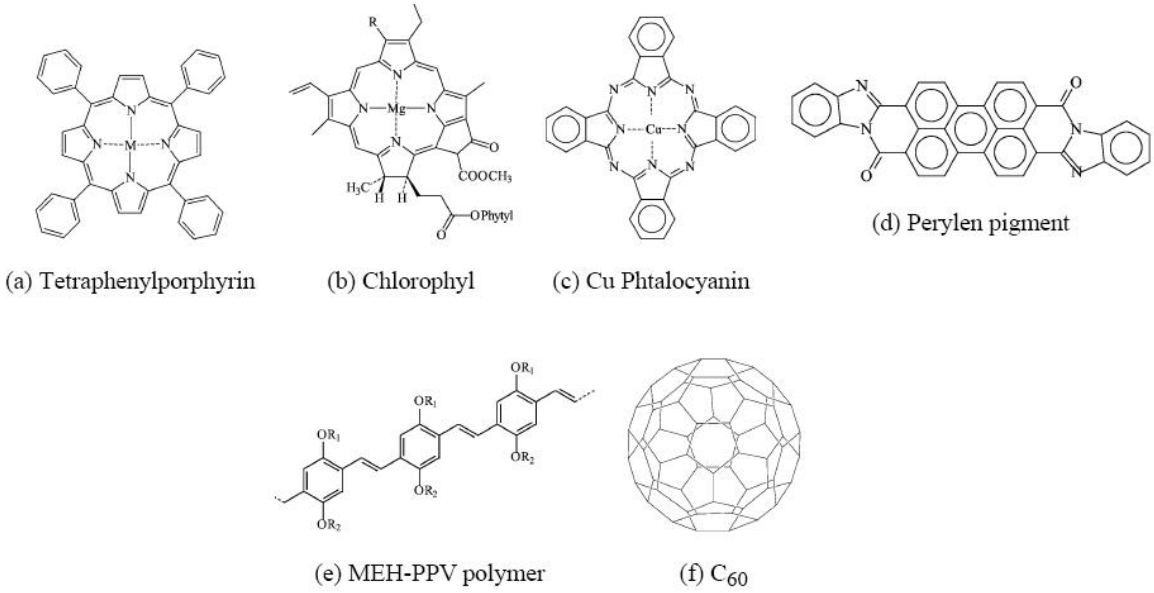

Fig. 8. Materials for organic solar cells.

The width of the charge generation layer for organic solar cells is small. In order to overcome this obstacle, the networks were modified with fullurene (C_{60}) particles. The efficiency of organic solar cell is relatively low. Only the modest solar conversion efficiencies of up to only 1% were reached until 1999. Efficiencies increased rapidly up to 3.3% with molecular flat-layer systems based on molecular organic single crystals made of iodine or bromine doped pentacene at Lucent Technologies [14].

3. **Dye-sensitized solar cells**

Enhancement of photovoltaic effects by dye can be dated back to the 19th century. In 1887, Dr. Moser in Vienna University reported the first dye sensitized photoelectric effect. In the 1960s, the first experiment was carried out using single crystal semiconductor electrodes immersed into dye solution. This device exhibited conversion efficiencies of less than 0.5% and poor long-term stability for applications in water splitting systems. In 1976, a breakthrough in conversion efficiency was reported by Tshubomura at al. using dyed high porosity multi-crystalline ZnO cell of energy conversion 1.5%. They also found that the iodide/triiodide redox shuttle system was outperforming to obtain high conversion efficiencies [16].

Since the mid 1980s, Gratzel's group in EPFL (Switzerland) has been the main driving force for development of dye sensitized solar cells. In 1991, they invented the cells of conversion efficiencies over 10% based on low-cost nano-porous TiO_2 deposited onto conducting glass [17].

3.1 Structure

The cell is constructed in a sandwich configuration (fig. 9). The working electrode is nanoporous TiO_2 placed on conducting glass and only separated by a thin layer of electrolyte solution (acetonitrile) from the counter electrode. The dye is chemisorbed onto the TiO_2 surface. The counter electrode is also made of conducting glass with a thin transparent platinum sputtered onto it to catalyze the regeneration process of mediator.

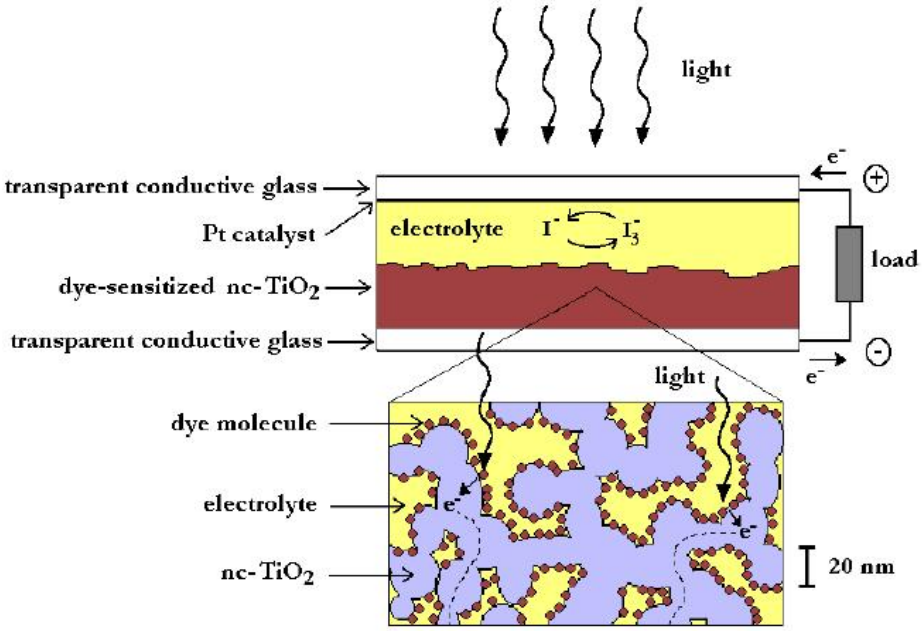

Fig. 9. The structure of dye-sensitized solar cells based on TiO_2 semiconductor.

3.2 Operating principle

A light photon enters the cell and traverses it until it is absorbed by a dye molecule. The dye will be promoted into its excited state (S*) from where it is energetically able to inject an electron into the TiO_2 conduction band. The electron can flow into an external circuit through a load in order that the energy can be utilized. After this, the electron, which now carries less energy, enters the cell via the counter electrode. From the counter/electrolyte interface it reduces the oxidized mediator (commonly the iodide/triiodide couple in very high concentrations of about 0.5M/0.05M). The remaining oxidized dye (S^+) on TiO_2 surface is then reduced back to its original state by the redox mediator ($S^+ + (3/2)I^- \rightarrow S + (1/2)I_3^-$), which completes the cycle (fig. 10) [18].

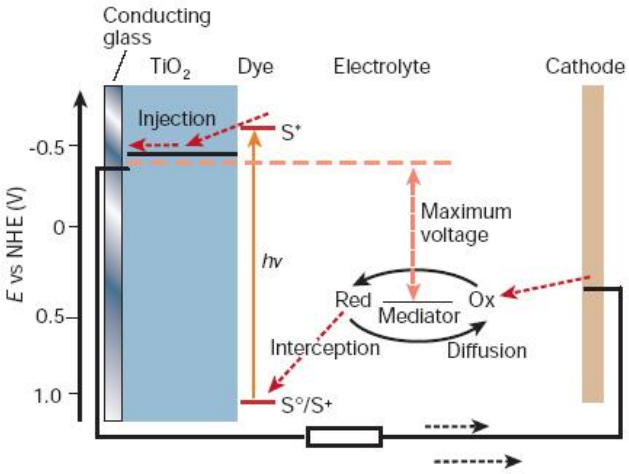

Fig. 10. Schematics of operating principles of dye-sensitized solar cells.

3.3 Conversion efficiencies

The overall conversion efficiency of the dye-sensitized solar cell is determined by the photocurrent density measured at short circuit (I_{sc}), the open-circuit photovoltage (V_{oc}), the fill factor of the cell (ff) and the intensity of the incident light (I_s).

$$\eta = \frac{I_{sc} x V_{oc} x ff}{I_s} \tag{6}$$

I_{sc}, V_{oc} are determined from the photocurrent-photovoltage curve of the cell (fig. 11). The fill factor was calculated as equation (7)

$$ff = \frac{IV}{I_{sc} V_{oc}} \tag{7}$$

where I, V were determined from the point of the curve the product of I and V is maximum.

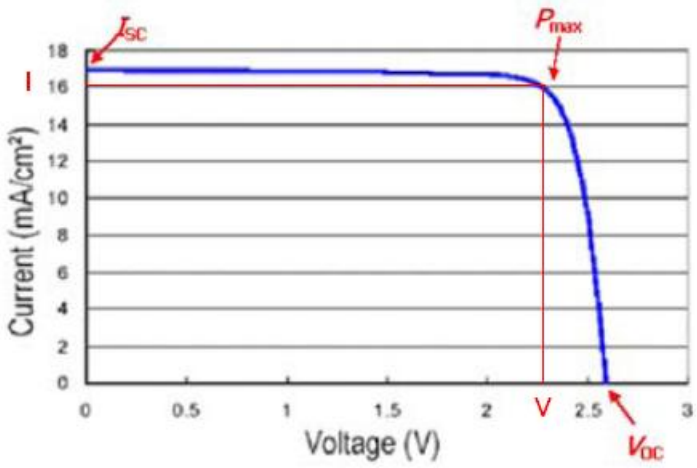

Fig. 11. The photocurrent-photovoltage curve of the cell.

4. Influential factors on conversion efficiencies

4.1 Dye

Many dyes were investigated for using in dye-sensitized solar cells. In 1993, Gratzel's group invented dye N3. It is very stable and the energy-to-electricity conversion efficiencies of the cells based on N3 reached 10%. The performance of *cis*-di(thiocyanato)bis(2,2'-bipyridyl-4-4'-dicarboxylate)ruthenium(II) (N3) was found to be outstanding and is unmatched by any other known sensitizer. The light harvesting efficiency (LHE) is 98% at the absorption maximum of the sensitizer and still 88% at the wavelength of half maximum height. The incident monochromatic photon-to-current conversion efficiency (IPCE) is impressive, the IPCE value exceeds 80% in the wavelength range between 480 and 600 nm, attaining a plateau of 100% between 510 and 570 nm. The electron inject from the excited complex into the semiconductor occurs at near 100% quantum yield. The sensitizer has sustained more than 10^7 turnovers without significant decomposition since beginning of illumination [19].

To obtain high conversion efficiencies, optimization of the short circuit photocurrent I_{sc} and open-circuit photovoltage V_{oc} of the solar cells is essential. The conduction band of TiO_2 is known to have a Nernstian dependence on pH. The fully protonated sensitizer upon adsorption transfers most of its protons to the TiO_2 surface, charging it positively. The electric field associated with the surface dipole generated in this fashion enhances the adsorption of anionic ruthenium complex and assists electron injection from excited state of sensitizer to the TiO2 conduction band, favoring high photocurrents. However the open-circuit photovoltage will be low due to the positive shift of the conduction band edge induced by surface protonation. If the sensitizer carries no proton at all, one expects a high value for V_{oc}, but low I_{sc}. Thus, there should be an optimal degree of protonation of the sensitizer that the product of I_{sc} and V_{oc} which determines the conversion efficiencies of the cell reach a maximum. On that reason, The performance of deprotonation levels of N3 ($Ru(dcbpyH_2)_2(NCS)_2$, $(Bu_4N)_2[Ru(dcbpyH)_2(NCS)_2]$ (N719) and $(Bu_4N)_4[Ru(dcbpy)_2(NCS)_2]$) (fig. 12) in solar cells was investigated and the doubly

protonated form (N719) exhibited power conversion efficiency superior to those of the other sensitizers [20]

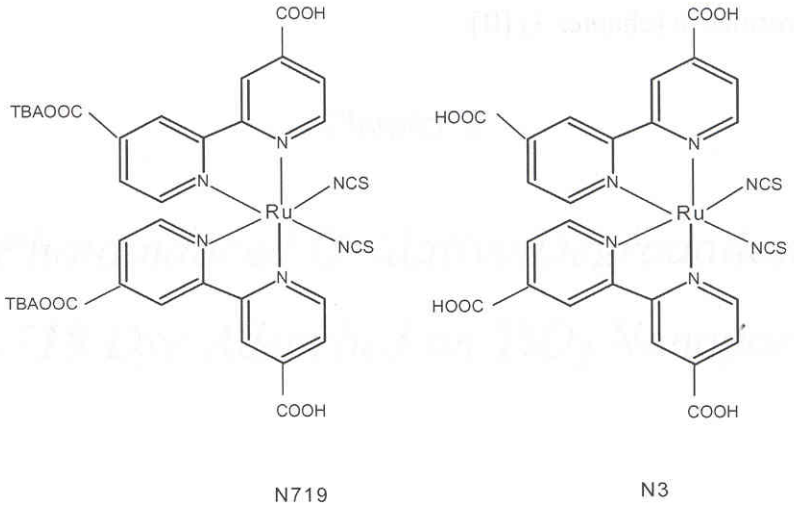

Fig. 12. Structure of N3 and N719

The main drawback of N3 is the lack of absorption in the red region of the visible spectrum and also relatively low molar extinction coefficient. New dyes with high extinction coefficient K8 and K9 (fig. 13) was synthesized. K8 showed IPCE 77% in the plateau region, and 66% even at 700 nm. K9 showed IPCE 73% in the plateau region and only 51% at 700 nm. The overall conversion efficiencies are 8.64 and 7.81 % for K8 and K9 [21].

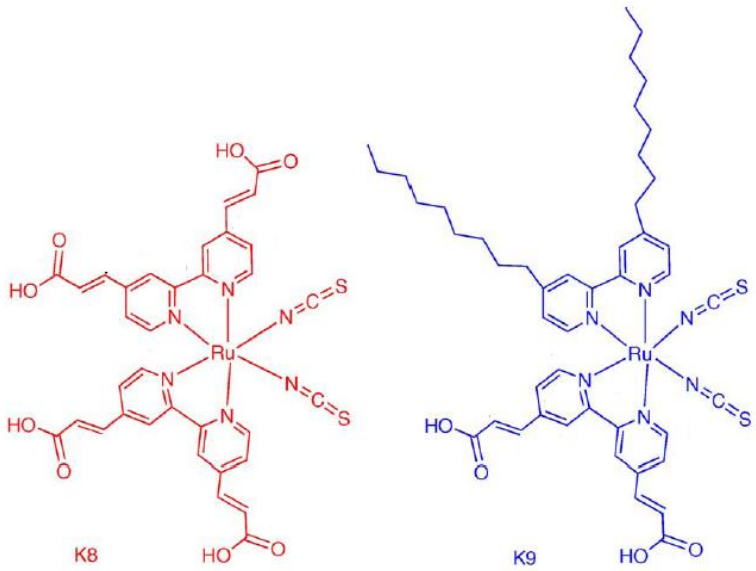

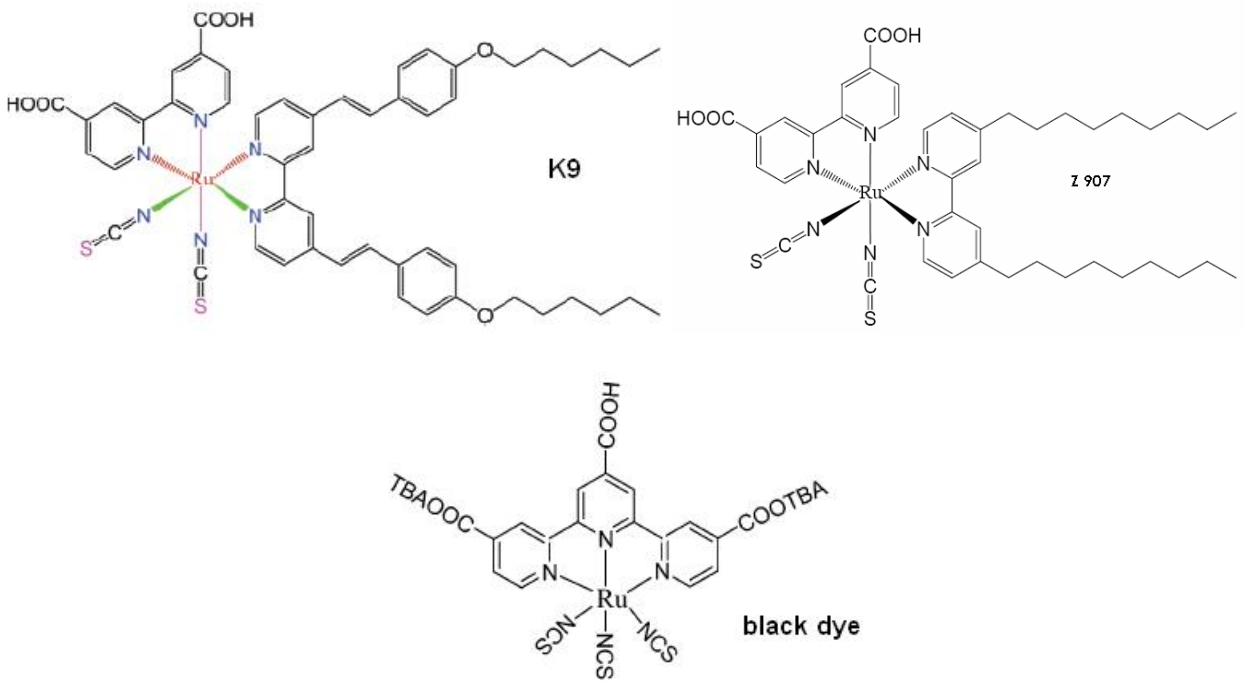

Fig. 13. Structure of K8, K9, K19, Z907 and black dye.

New dye K19 (fig. 13) was synthesized, it showed the extinction coefficient 18.2×10^3 M^{-1} cm^{-1} higher than Z-907 (12.2×10^3 M^{-1} cm^{-1}), N719 (14.0×10^3 M^{-1} cm^{-1}). The overall conversion efficiency (7.0%) is higher than Z907 (6.0%) and N719 (6.7%) in the same condition of preparation of solar cells. This dye lasts constantly after 1000h of light soaking at 60^{o}C without decomposition [22].

The best dye sensitizer reported so far is the black dye (fig. 13) with visible absorption extending into the near-IR region up to 920 nm with IPCE 80%, producing an overall efficiency of 10.4% [23].

4.2 Semiconductor

Nanorods TiO_2 (diameter 5-10 nm, length 100-200 nm, S_{BET} 203 m^2/g) is higher photocatalytic than P25 (70% anatase), ST01, JRC01 (anatase), JRC03 (rutile) in catalysing I^- -> I_2 with UV. The overall conversion efficiency of cells based on this material is 7.12%

compared with 5.82% for P25 [24]. Mix-solvent-thermal synthesis of anatase (little rutile) 10 nm from $TiCl_4$ gives higher conversion efficiency of cells 9.13% compared with 8.49% (TiO_2 from Solaronix). Thinner film 6 μm has the same optical density as 10 μm Solaronix film [25].

The ZnO semiconductor is also used in solar cells. But the conversion efficiency of solar cells based on ZnO is relatively low. A 30 μm thick ZnO cell with dye N3 has overall conversion energy efficiency 2% and IPCE 50-60 % at 540 nm [26].

4.3 Additive

Charge carriers can be trapped in localized energy levels just below the conduction band edge well-established as a Ti^{3+} (3d) state. The implication of electron trapping in the efficiency of the dye-sensitized solar cell can be multifold. Slow time response of the photocurrent but not to recombination losses lead to a lower position of the quasi-Fermi level for the electrons during illumination and a reduced photovoltage. Electrons are trapped may act as an intermediate in the reduction of triiodide by conduction band electrons, lead to a lowering of photocurrent and a decrease in the photovoltage. One of the key issues to improve the efficiency of dye-sensitized TiO2 solar cell is to reduce the rate for triiodide reduction, i.e. to block the surface states below the conduction band edge. Since the photocurrent quantum yield is practically unity, this will merely affect the photovoltage. Treatment with 4-tert-butylpyridine on TiO_2 surface increases the photovoltage by about 0.3 V, corresponding to a 5.5×10^4-fold decrease in the rate constant for triiodide reduction [27].

4.4 Charge transfer

Electron injection from coumarin into conduction band around 160 fs. Cation radical formed with yield of 100%. Charge recombination occurs over several microseconds. $k_{inj}/k_b > 10^3$, in some cases exceeds one million. Why the rate of back-reaction is so much smaller than that of forward reaction. Recapture of conduction band electron has large driving force placing this reaction in inverted region where the rate drops with increasing exothermicity. Entropic factor, in 12 nm size TiO2 particles the electron is delocalized over 3000

conduction band states. If only one sensitizer cation available at surface, the back-reaction decrease entropy amount of 16 cal $K^{-1}mol^{-1}$. In addition, carboxylate groups interact directly with surface Ti (IV) ions resulting in good electronic coupling of π* molecular orbitals of the carboxylated bipyridyl ligand with 3d orbital of conduction band of TiO_2. By contrast, the back-reaction involves the small overlap between d orbital localized on Ru (III) and TiO_2 conduction band.

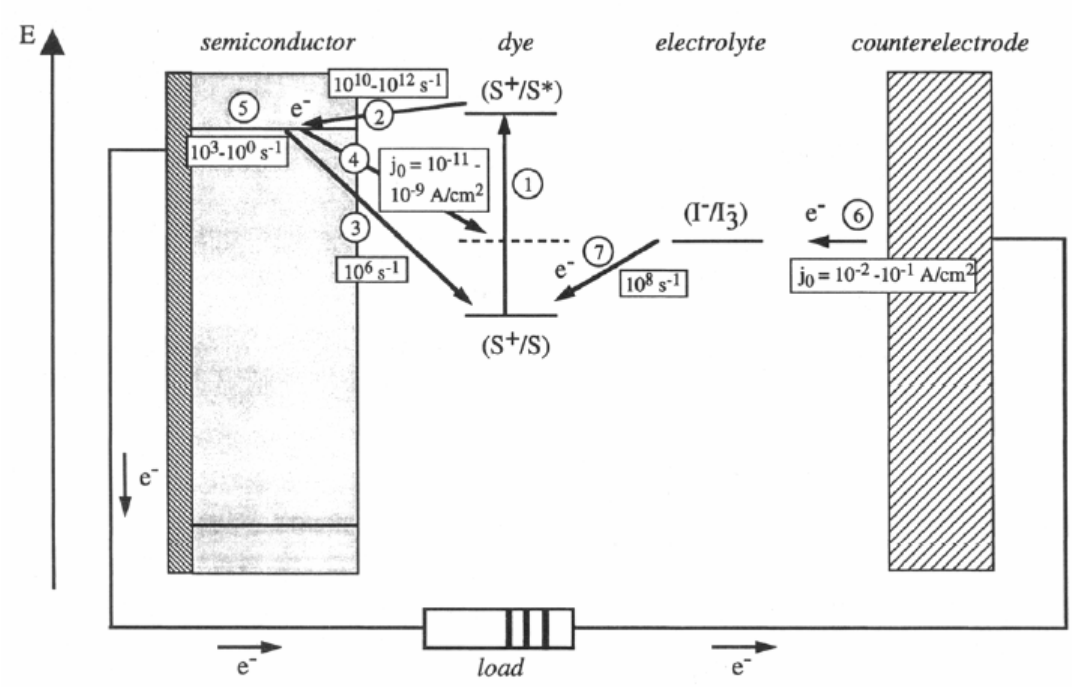

Fig. 14. Kinetics of charge transfer processes in solar cells.

The rate constants of the reaction steps for Ru complex photosensitized TiO_2 solar cell. Following light absorption of Ru dye (1), the electron injection into the conduction band (2) is in picosecond range with quantum yield near 100%. The rate of back reaction (3) is much smaller, typically $\tau \approx 1$ μs. another recombination process is reduction of triiodide in electrolyte by conduction band electrons (4), exchange current density j_o, 10^{-11}-10^{-9} A/cm^2. The electron movement in the nanocrystalline TiO_2 electrode to the back-contact (5) is in millisecond to second range. The exchange current density j_o for reduction of triiodide at the counter electrode (6) 10^{-2}-10^{-1} A/cm^2. The reduction of the oxidized dye by iodide (7) occurs on 10^{-8} s (fig. 14) [27].

5. Stability of dye-sensitizer solar cells

5.1 Degradation of DSSCs

DSSCs have been paid much attention due to its low cost and high efficiency. However, there are few of degradation research of DSSCs. Hagfeldt'g group used UV-Vis and IR to investigate the degradation of N719 bound to TiO_2 particles in DSSC. They found that the thiocyanate ion ligand is the most sensitive part of the dye, N719 when adsorbed onto TiO_2 in DSSC. This ligand is lost in air, at temperature equal to and about 135^oC, in electrolyte and possibly upon UV radiation. The loss of NCS^- in air was accelerated under visible illumination. In complete solar cells, I_3^- was found to exchange the NCS^- ligand, together with water in electrolyte, the NCS^- ligand can be exchanged with H_2O or OH^- and was accelerated under visible illumination [28]. The complex between NCS^- and I_2 was observed by Resonance Raman Scattering in DSSC of N719 (8). The dye after loss of NCS^- is proposed to be a *cis*-bis-(iodo)bis(2,2'-bipyridine-4-carboxylic acid, 4'-carboxylate) ruthenium(II) complex. The role of additive 4-tert-butylpyridine suppresses the loss of NCS^- from the dye (equation 9, 10, 11). Mechanisms of the processes were shown [29]:

$$I_2 + SCN^- \rightarrow I_2SCN^- \quad (8)$$

$$(dcbpy)_2Ru(SCN)_2^{2-} + 2I_3^- \rightarrow (dcbpy)_2RuI_2^{2-} + 2I_2SCN^- \quad (9)$$

$$(4TBP) + I_3^- \rightarrow (4TBP)I_2 + I^- \quad (10)$$

$$(4TBP) + I_3^- \rightarrow (4TBP)I^+ + 2I^- \quad (11)$$

Torben Lund' group has investigated the degradation of N719 bound to TiO2 particles in acetonitrile [30]. After photolysis with laser light, the dye and degradation products was extracted and analyzed by HPLC-UV-MS. They found four main degradation products on the chromatograms (fig. 15): $RuL_2(NCS)(ACN)^+$ at 7.23 min, $RuL_2(NCS)(NC)$ at 6.77 min, $RuL_2(NCS)(H_2O)^+$ at 6.43 min and $RuL_2(NC)_2$ at 4.77 min. The peak at 9.22 min and 8.68 min are $RuL_2(NCS)_2$ and its isomer $RuL_2(NCS)(SCN)$ (from the starting N719 without degradation).

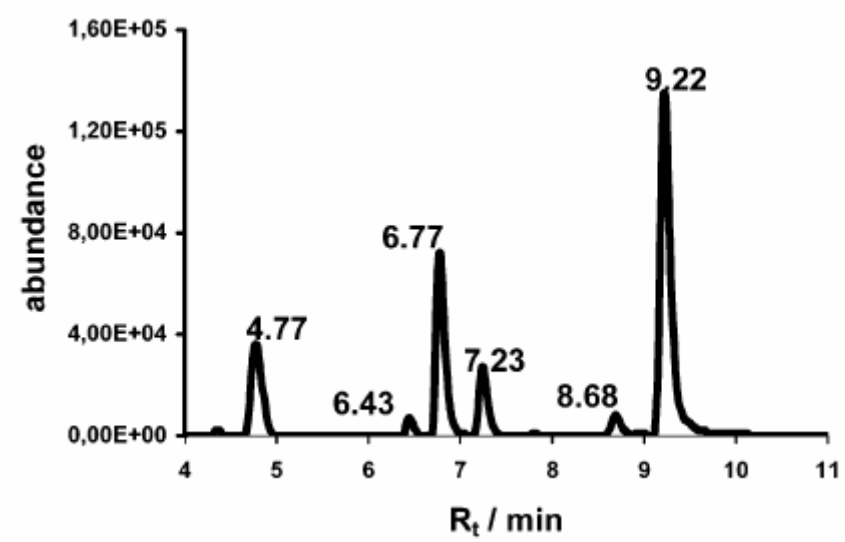

Fig. 15. Chromatogram of degradation of dye N719

The group has also studied the degradation of N719-TiO_2 system in the present of additive 4-tertbutylpyridine in acetonitrile. The substitution product $Bu_4N^+RuL_2(NCS)(4\text{-}TBP)^-$ was observed [31].

5.2 Lifetime

Gratzel has estimated DSSCs' lifetime of 20 years. However, only Torben Lund's group has established the base for calculation of DSSCs' lifetime based on a model system accelerated by photolysis experiments [30]. On the model system, solution of dyed-TiO_2 colloidal in acetonitrile was irradiated with laser light coupled with photon counting device. The degradation products were extracted from TiO_2, and analyzed by HPLC-UV-MS. The processes occurred in photolysis was shown in fig. 16.

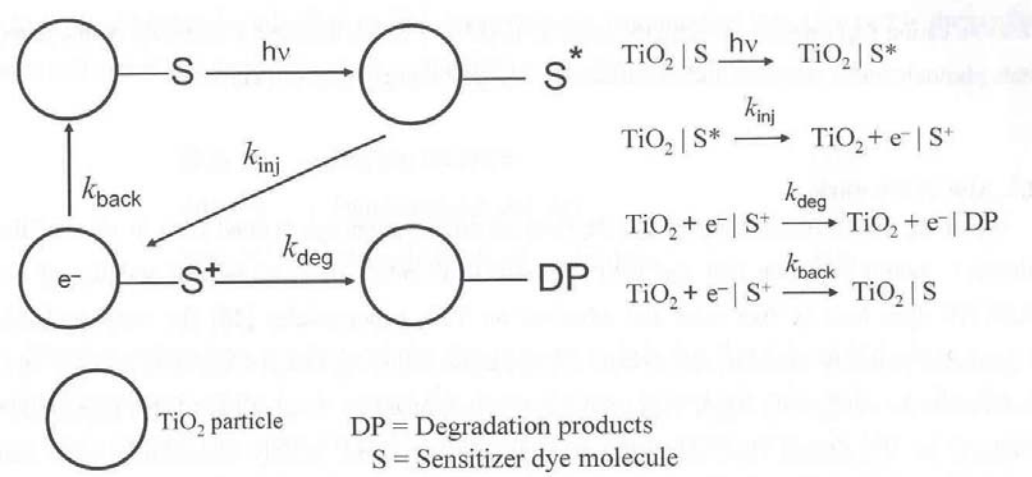

Fig. 16. The processes occurred in photolysis

When the dye absorbed a photon, it went into the excited state. The excited state injected rapidly electrons into conduction band of TiO2 to become oxidized state. The excited state can recombine with electrons by k_{back} and degrade into degradation products by k_{deg}. Because the electron injection is very quick, $k_{inj} \sim 10^{13}$s, the efficiency of electron injection is nearly 100%. The quantum yield of degradation processes can be calculated by following equations:

$$\phi_{deg} = \frac{\sum n_{deg}}{n_p} \quad (12)$$

$$\phi_{deg} = \frac{k_{deg}}{k_{deg} + k_{back}} \sim \frac{k_{deg}}{k_{back}}; \ k_{back} >> k_{deg} \quad (13)$$

$\sum n_{deg}$ was determined by analyzing quantitatively of chromatograms; n_p was calculated from the photon counting device; Φ_{deg} was the slope of straight line when plotting the total amount of degradation products vs. the mole of photon; k_{back}, the rate of back electron transfer was measured by photoinduced spectroscopy. We can calculate kdeg by equation (14):

$$k_{deg} = \Phi_{deg} k_{back} \quad (14)$$

The turnover number N of dye can be calculated by equation (15):

$$N = \frac{k_{reg}}{k_{\deg}}[I^-] \quad (15)$$

where k_{reg} is the rate of regenerative electron transfer between iodide and Ru^{III} complex ($S^+ + (3/2)\ I^- \rightarrow S + ½\ I_3^-$). Because the k_{reg} was not the same in literature, it was necessary to determine this number to calculate the accuracy lifetime.

6. **Aim of thesis**

The degradation of the solar cell dye N719 was previously investigated in Torben Lund's group. On the model system, degradation products of N719 bound to P25 Degussa TiO_2 was identified and the degradation rate k_{deg} was also calculated. In this thesis, we aimed to determine degradation rates of N719 on different kinds of TiO_2 by the model system. The effect of anatase/rutile ratio and oxygen amount on degradation rates was studied.

At the second part of thesis, we wanted to build the solar cells by the procedure of Anders Hagfeldt's group. Also, we aimed to determine the conversion efficiencies of the solar cells made of different kinds of TiO_2 semiconductor.

Experiments

1. TiO_2 Characterization

1.1 X-ray

The crystalline and structural composition of different TiO_2 samples (P25, ST01, ST21, ST31 and ST41) was investigated by using X-ray diffraction. Apart from 5 raw commercial types of TiO2, their heated samples at different temperature (450, 550, 900^oC) were also characterized. The X-ray diffractions were performed with a Siemens D500/501 diffractometer using Cu-Kα (λ=0.1540 nm) radiation with Ni filter. The diffractometer was set up at 40 mA, 40 K, a step size of 0.04^o/s and collection angle 2θ from 2^o to 80^o.

1.2 SEM

Surface characteristics of TiO_2 samples were observed by scanning electron microscope JEOL Model 6320F. A SEM has a E-gun. We can pull the electrons out of a filament by setting a few KV (Kilovolt) voltage and accelerate them from 0 KV to 30 KV. These electrons go first through a condenser lens and then through a objective lens, then through a aperture (a opening) and finally reach to our specimen which is the silicon wafer covered by TiO_2 particles by doctor blading technique. The electrons scatter back again. Some of them with high energy scatter back from the surface (called back scatter electrons) and some of them go a bit in the sample and back again (called secondary electrons). The signal from secondary electrons detected by detector are amplified and sent to the observation Cathode Ray Tube (the screen). It was these secondary electrons we used to observe the samples. The acceleration voltages at 30 KV and 15 KV were used.

2. Degradation rate

2.1 Chemical actinometry [32, 33]

We used chemical actinometry for calibration of the counting device. Aberchrome 540 (fig. 17) is well suited for chemical actinometry within the ranges 310-370 nm and 435-545 nm. In the UV-Vis spectra, the dash curve corresponds to form 1 and the solid curve for form 2.

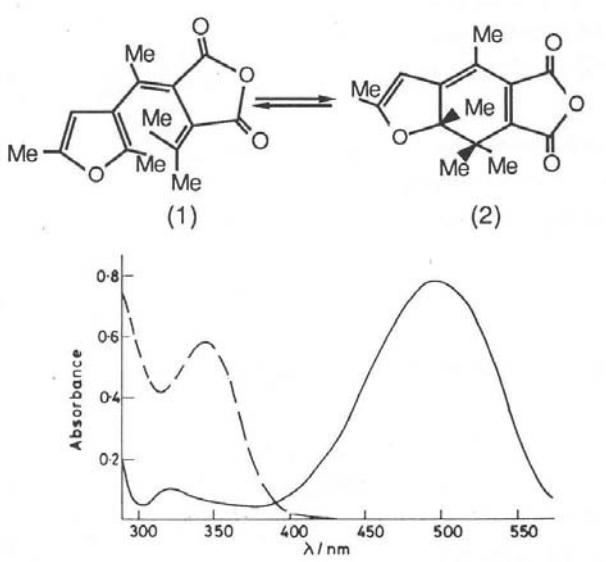

Fig. 17. Aberchrome and its UV spectrum

25 mg of Aberchrome 540 was dissolved in 20 ml of toluene. 3 ml of the solution was pipetted into a cuvette. The cuvette of colorless solution was radiated with a Xenon Lamp ($\lambda \approx 350$ nm) for nearly 4 minutes and it transformed to the red solution. Then we measured the absorbance of the red solution with UV-Vis spectrometer using a wavelength $\lambda = 494$ nm, the absorbance is about 2.

The calibrating system consists of the laser equipment connecting with the photon counting system (fig. 18). The photon counting system comprises of a cuvette holder and a black box in which there are a light splitting system, which 90% of the light was directed toward the sample and 10% to a photodiode. The electrical response of the diode was monitored and integrated electronically

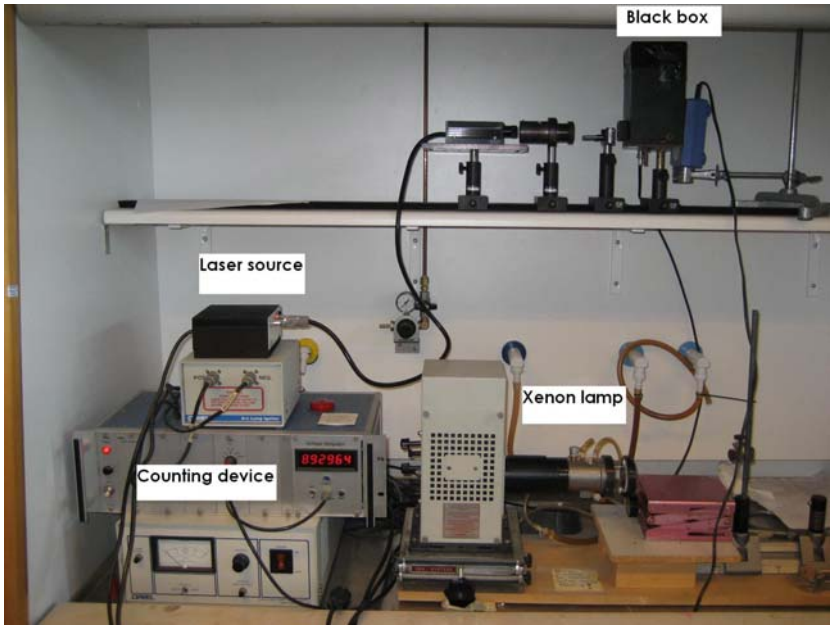

Fig. 18. The photolysis system.

After the absorbence of the red solution was measured, the cuvette was placed in the black box of the counting device and radiated with 532 nm laser light for a defined count number. The cuvette was taken out and measured the absorbance at λ = 494 nm. Then we repeat to radiate with increasing count number and measure the absorbance for many times until the absorbance approximate to 1.

The photon flux I can be calculated form the following equation (16):

$$I = \frac{\Delta A.V.N}{\Phi.\varepsilon.t} \tag{16}$$

where ΔA is the absorbance difference; V is the volume of solution radiated; N is the Avogadro number; Φ is the quantum yield for decoloring at 532 nm; ε is the molar extinction coefficient for Aberchrome 540 at 494 nm; t is radiation time.

The counting number CN relates to the photon flux I as following equation (17):

$$CN(t) = \alpha I_E t \tag{17}$$

Where α is constant related to the laser light intensity going into the cuvette and the counting number from the photon counting system, I_E is the laser light intensity in Einstein.

Combining two equations, we obtained:

$$CN = \frac{V.N.\alpha}{\Phi.\varepsilon}\Delta A \tag{18}$$

where V = 3 ml, N = 6.023×10^{23}, ε = 8200×10^{3} ml mol^{-1} cm^{-1}, Φ was calculated as following equation: $\Phi = 0.178 - 2.4\times10^{-4}\times\lambda$; with λ = 532 nm, Φ = 0.05 [34].

Plotting CN = f (ΔA), we got the straight line (fig. 19). From the slope of the line, we obtained the value of $\alpha = 2.97\times10^{-15}$.

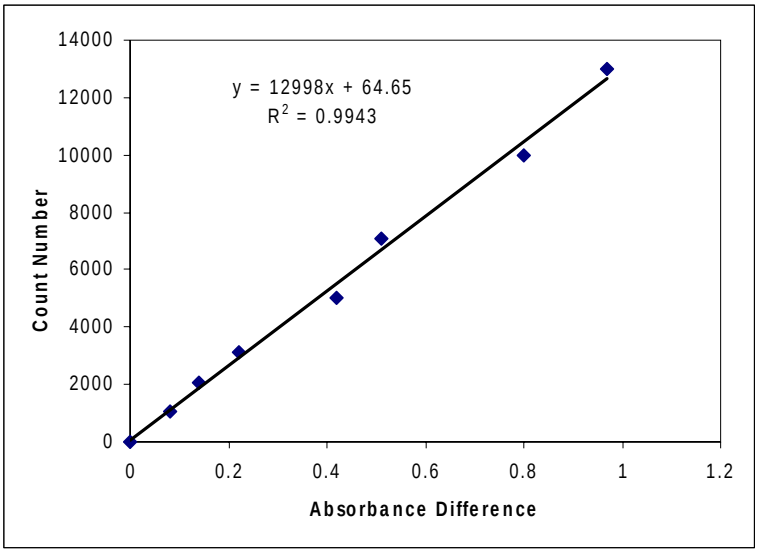

Fig. 19. The straight line of count number vs. ΔA

The value of α helps us calculate the light intensity and the mole of photons shining through the cuvette in photolysis experiments. To calculate the laser light intensity I, the light was irradiated through the cuvette in a period of time t, we also knew the counting number CN. Hence,

$$I = \frac{CN.h.c}{\alpha.S.t.\lambda} \tag{19}$$

where h is Planck constant 6.63×10^{-34} J.s, c is light velocity 3×10^{8} m s^{-1}, λ is the wavelength of laser light 532 nm. S is the area of light cycle shining on the cuvette, the diameter of the light cycle is 1 cm. In all photolysis experiments, we used the laser light without a filter, the light intensity calculated is 9.2 mW/cm^2. The mole of photon n_p in photolysis experiments was calculated as following equation (20):

$$n_p = \frac{CN}{\alpha.N} \tag{20}$$

2.2 Dye adsorption capacity

In this experiment section, we measured the maximum dye adsorption capacity of many TiO_2 samples. From these results, we can determine the amount of dye needed to use in photolysis experiments. 6 samples TiO_2 was use as P25, P25 heated at 900 ^oC (Degussa), ST01, ST21, ST31, ST41 (Ishihara Sangyo Kaisa company).

4.23 mg of N719 was dissolved in 20 ml of absolute ethanol. The molarity of solution is 1.78×10^{-4} mol/L. 15 mg of each TiO_2 sample was stirred magnetically in 3 ml of this solution in test tube for 24 hours. After centrifuging, the supernatant liquid along with the initial N719 solution was run on HPLC-UV-MS system to determine the amount of N719 adsorbed on TiO_2. The maximum dye adsorption capacity of TiO_2 samples a_{max} (amount of N719 in mg adsorbed on 1 mg of TiO_2) was calculated as the following expression (21):

$$a_{\max} = \frac{m_{N719}.V_2.(S_1 - S_2)}{V_1.S_1.m_{TiO_2}} \tag{21}$$

where m_{719} = 4.23 mg, m_{TiO2} = 15 mg, V_1 = 20 ml, V_2 = 3 ml; S_1 and S_2 are the areas of N719 peak on the chromatograms before and after adsorption. The a_{max} value of different TiO_2 samples was expressed in the table 1:

Table 1: The maximum adsorption capacity of TiO_2 samples

Samples	$\mathbf{a_{max}}$
P25	0.040
ST01	0.032
ST21	0.027
ST31	0.036
ST41	0.014
P25 at 900 ^oC	-

As we can see, the dye adsorption capacity of ST41 and P25 heated at 900 ^oC were so small, they would not be relevant to using in DSSCs. Therefore we did not use them in photolysis experiments.

2.3 Preparation of dyed-TiO_2

From the results of dye adsorption capacity, we used 4 types of TiO_2 (P25, ST01, ST21 and ST31) in photolysis experiments. For each kind of TiO_2, 600 mg TiO_2 was magnetically stirred in 250 mL of an N719 (Solarnix) dye solution ([N719] ~ 6.0×10^{-5} mol/L) in absolute ethanol. After 24h, solvent was removed by rotary evaporation and the red-colored TiO_2 particles were transferred into a brown bottle and stored in the dark.

2.4 Dark degradation

In this section, we determined amount of degradation products without shining the laser light. For each kind of TiO_2, 12 mg of dyed TiO_2 was put into a test tube. The solution containing 1 ml of ethanol and 2 ml of NaOH 0.1 M was added to extract the dye bound to TiO_2 particles. After centrifuging, the supernatant liquid was taken out with a plastic syringe and pumped into a HPLC vial through a 0.2 μm plastic filter. The plastic filter was used to prevent TiO_2 particles from going into the vial. Then 15 μl of formic acid was added to the vial to acidify the solution, then the vial was run with HPLC-UV-MS.

We also studied the amount of degradation products on time. 5 samples of dyed-P25 colloidal solution in test tube were wrapped in aluminium foil and left for different times (3,

24, 48, 72 and 120 h). Each sample consists of 12 mg of dyed P25 and 3 ml of acetonitrile. At defined moment, one sample was taken out to extract the dye bound to TiO_2 with the same procedure above, acidified and run with HPLC-UV-MS system.

2.5 Photolysis

We investigated the degradation rates of the dye adsorbed on different kinds of TiO_2 (P25, ST01, ST21, ST31). For each kind of TiO_2, the dyed TiO_2 powder samples (12 mg) were also placed into a cuvette containing 3 mL of acetonitrile. The mixture was degassed with argon gas for 30 minutes, then sonication for 1 h. The cuvette containing the dyed colloidal TiO_2 solution was placed into the black box of a photon-counting device. The sample was magnetically stirred and simultaneously irradiated with continuous unfiltered laser light (532 nm) with an intensity of 9.2 mW/cm^2 for the durations to obtain light doses at 100, 200, 300, 400, 500, 600 thousand of counts.

To investigate the effect of oxygen on degradation, two conditions: getting rid of oxygen and saturating with oxygen were studied. To get rid of oxygen, the cuvette comprising 3 ml ACN and 12 mg of dyed P25 was frozen with liquid nitrogen, sucked with vacuum pump, dipped in ethanol, then frozen and sucked again for 4 times (figure 20). To saturate with oxygen, the cuvette containing 3 ml of ACN and 12 mg of dyed P25 was saturated with oxygen gas for 30 minutes. The free and saturated oxygen samples were sonicated for 1 h, then irradiated in the same system with the same light doses.

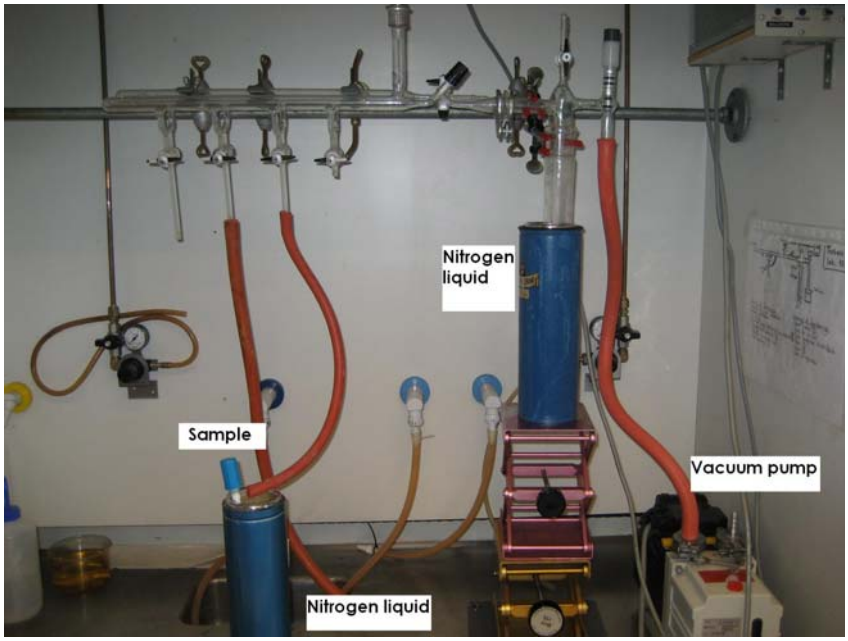

Fig. 20. The system for disposing of oxygen

The dyed colloidal TiO_2 solution after photolysis was centrifuged. The colorless supernatant liquid was removed by degassed with nitrogen gas at 50 ^oC, then a solution comprising of 1 mL of absolute ethanol and 2 mL of 0.1 M NaOH was added to extract the dye and its degradation products bound to the TiO_2 particles. Centrifuging again, the red supernatant liquid was transferred into an HPLC vial by a plastic syringe and a 0.2 μm plastic filter, 15 μL of concentrated formic acid was added to acidify the solution and the vial was stored in the refrigerator to analyze with HPLC-UV/Vis-MS when necessary.

2.6 HPLC-UV-MS

The LC-MS instrument was equipped with a UV diode array detector with a 5-cm flow cell in series with an MS detector (figure 21). The HPLC instrument was a TSP Spectra System equipped with an AS3000 auto sampler, a P4000 gradient pump, a vacuum degasser, and a UV 6000 LP diode array detector. Separation was performed with a linear gradient program starting with 100% A (5% acetonitrile + 94% water + 1% formic acid) ending after 21.6 min with 100% B (acetonitrile). Elution with 100% B continued for further 10 min, followed by a return to 100% A after further 5 min. The flow rate was 0.2 mL/min. The analytical column was a 50-mm Xterra MS RP C18 column from Waters with an i.d. of 2.1 mm. The

mass detector was an LCQ-Deca ion-trap instrument from ThermoFinnigan equipped with an electrospray ionization interface (ESI) run in positive mode. A positive potential (+4.5 kV) was applied to the silica needle, while the other details of the setup were as follows: discharge current 19 – 20 mA, capillary voltage 23 V, capillary temperature 350 ^{o}C, tube lens offset 5 V, and sheath gas (N_2) and auxiliary gas (N_2) 78 and 45 arbitrary units, respectively. UV-Vis absorptions were recorded between 400 and 600 nm. The ion trap was run in the data-dependent MS scan mode. The scan event was obtained in the 400 – 800 m/z interval. The parent mass list was 643.1, 648.1, 674.9 and 706, while the reject mass list was 547, 569, 585, 591, 613, 629, 636 and 592. The isolation m/z width was 6, the normalized collision energy was 35, the activation time was 30 ms, and the minimum signal required 10^5 counts. Xcalibur 1.3 LCQ software controlled the chromatographic and mass spectrometric analysis.

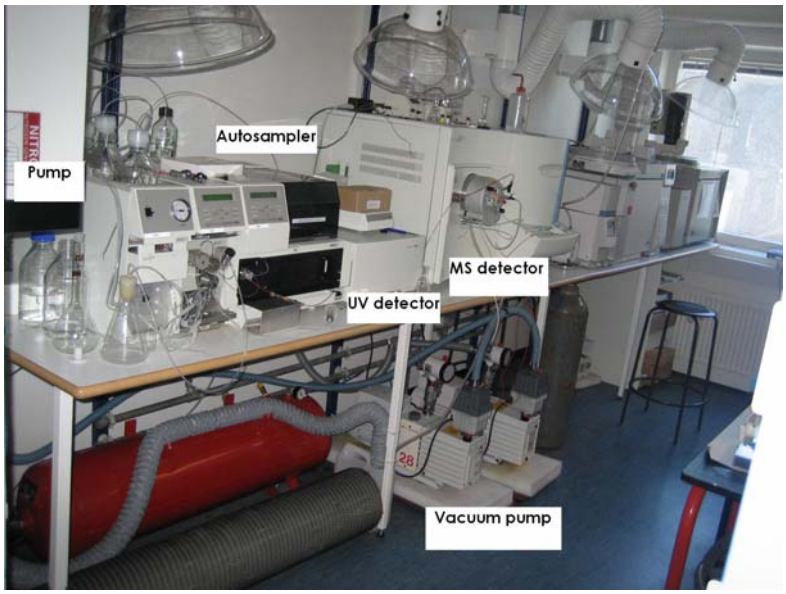

Fig. 21. The HPLC-UV-MS system

To investigate the effect of capillary temperature on mass spectra, we run some samples with the same method above, only changed the capillary temperature to 250 ^{o}C.

2.7 Photoinduced Absorption Spectroscopy

A 1.0-mm path-length cuvette containing the dyed TiO_2 sample was illuminated with chopped light from 532-nm He-Ne continuous wave laser. Resulting absorption changes at 800 nm was probed with light from a filtered tungsten-halogen lamp ($\lambda > 715$ nm), using a monochromator, a Si-detector, and a lock-in amplifier set at chopping frequency (range 400 to 4 Hz). Neutral density filters were used to attenuate the laser beam. Time constants were obtained with a nonlinear, least-squares fit of the frequency domain data.

3. Building of dye-sensitized solar cell

3.1 Preparation [35]

In this section, we prepared the ASC/NSC sealed glass cells on 0,785 cm^2 round design with 4 kinds of TiO_2. The 1.5x2.5 cm pieces of the fluorine-doped tin oxide TCO glass (Hartford Glass Company, Inc.) was used both for working and counter electrode. The sealing glass (very thin glass) was cut into 1.5x1.5 cm pieces. All pieces of glass are cleaned on ultrasound bath in ethanol over night or at least for a couple of hours. 50 mg of N719 was dissolved in 100 ml of absolute ethanol and stirred magnetically over night. The 5 mM solution of H_2PtCl_6 was prepared by dissolving 20 mg of H_2PtCl_6 in 10 ml of 2-propanol. The recipe of electrolyte solution: 50 mL electrolyte-solution in acetonitrile or 50 mL in 3-methoxypropionitrile containing I_2 0.05 M, LiI 0.1 M, tetrabutylammonium iodide 0.6 M and 4-tertbutyl pyridine 0.5 M. The components were dissolved completely through sonication.. The TiO_2 colloidal solutions was stirred magnetically, and followed by sonication with 2 hours. The TiO_2 colloidal solution was received from Anders Hagfeldt's group (Royal Institute of Technology, Sweden). This solution consists of HNO_3 0.5 M, ratio of TiO_2 and PEG equal to 1:1.

We also built the cells on our TiO_2 samples, the colloidal solution of each kind of TiO_2 consists of 0.1 g of polyethylene glycol (PEG) and 0.2 g of TiO_2 in 2 ml of mili-Q water [36].

Working Electrode: the TCO glass was fixed onto the table with conducting side up (using Ohm meter to determine the conducting side). The 50 µm thick Scotch tape mask was holed in diameter of 1 cm, then applied onto the conducting side of the glass. The TiO_2-mixture was cover onto the hole by doctor blading. The mask was removed and TiO_2 was got dry for 20 minutes**.** The electrodes were sintered in an oven for 30 minutes at 450°C-500°C. Afterwards the electrode must cool down to around 80°C before it can be touched, it might crack if it's too hot. The electrode immediately put in a bath of the N719 solution in absolute ethanol over night.

Counter Electrode: Two holes were drilled with diamond-coated drill, speed 9 on the "Dremel Multipro 395VP". The holes must be drilled from the conducting side, and they should be located about 2 mm from each short side of the film in the finished cell. To avoid overheating a constant flow of water was applied to the drill when drilling. The drill is Ø 1 mm purchased from www.lopacki.com. Then, the glass was cleaned and stored in ethanol over night. After that, the conducting side was covered with 5 mM solution of H_2PtCl_6 in 2-propanol, about 10 µl from a piece of glass. Let it dry for a couple of minutes. The electrode was sintered in the oven for 30 minutes at 380 °C. Afterward the electrode must cool down to around 80°C. The surlyn frame 1601 cleaned in ethanol is placed on the counter electrode and heated till the surlyn frame is attached to the counter electrode.

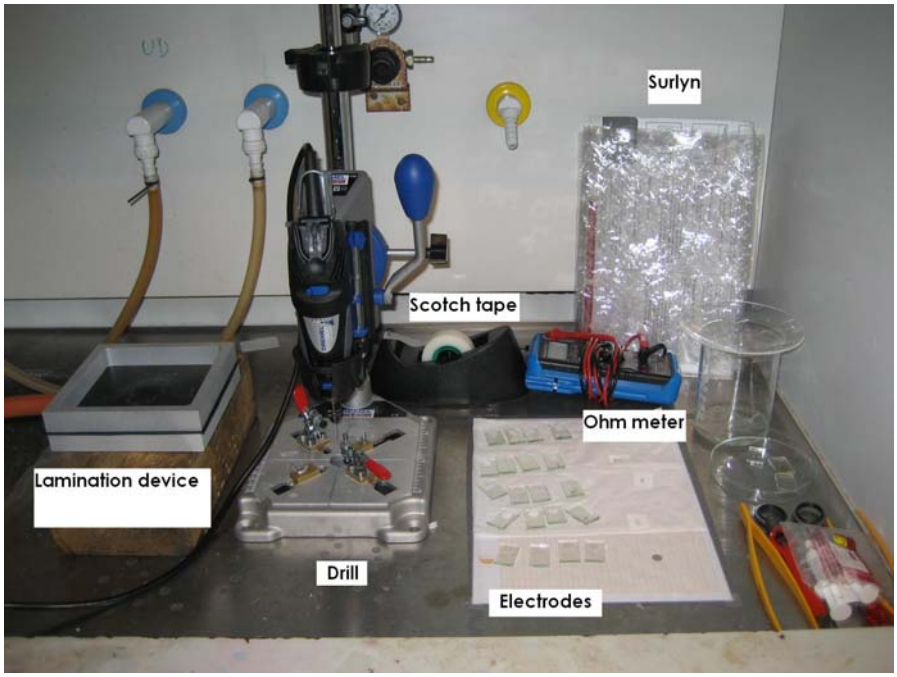

Fig. 22. The toolkit for preparation of DSSCs

Assembling the solar cell: The counter electrode was fixed on top (with a clamp), the conducting side must be towards the working electrode. Then, the assembled electrodes were put in the lamination device in 2 minutes of vacuum (by water flow) at 120 °C. Let it cool down for a couple of minutes. The cell was filled with the electrolyte solution by using the micropipette. A piece of surlyn 1702 in the same size as the sealing glass was put onto the hole, then put the covering glass onto the surlyn, and then laminate. The lamination time was about 2 seconds to avoid the electrolyte from boiling. Make sure no air bubbles are formed under the surlyn by laminating on a few different spots around the hole. The conductive epoxy was applied on the conducting side of each electrode, it was put as close to the area as possible, without short-circuiting the cell. The cells accomplished was shown in fig. 23.

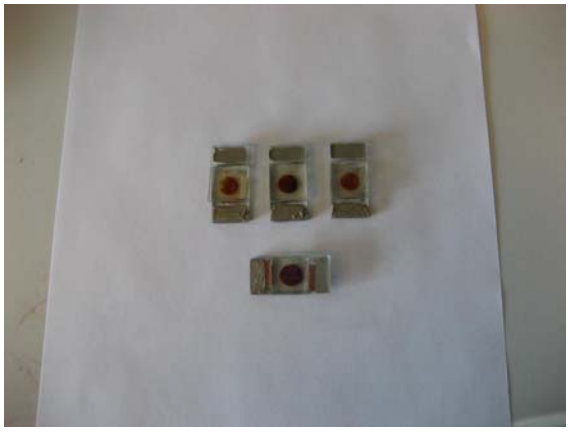

Fig. 23. The dye-sensitizer solar cells

Results & discussion

1. TiO_2 Characterization

1.1 X ray diffraction

X-ray diffractions of 5 unheated types of TiO_2 were presented in figure**.** The peaks at $2\theta = 25^o$ characterized to anatase form and the peaks at $2\theta = 27^o$ specified to rutile form. As we see on the X-ray diffractions (fig. 24), 4 kinds ST01, ST21, ST31 and ST41 consist of pure anatase. X-ray pattern of P25 contains a small peak for rutile, the amount of rutile phase is estimated approximately 20%.

The X-ray patterns of P25 and ST01 at different temperatures was shown in figure. Until 550^oC, there is no phase transition in two TiO_2 samples. At 900^oC, the composition of two TiO_2 samples contains only the rutile phase.

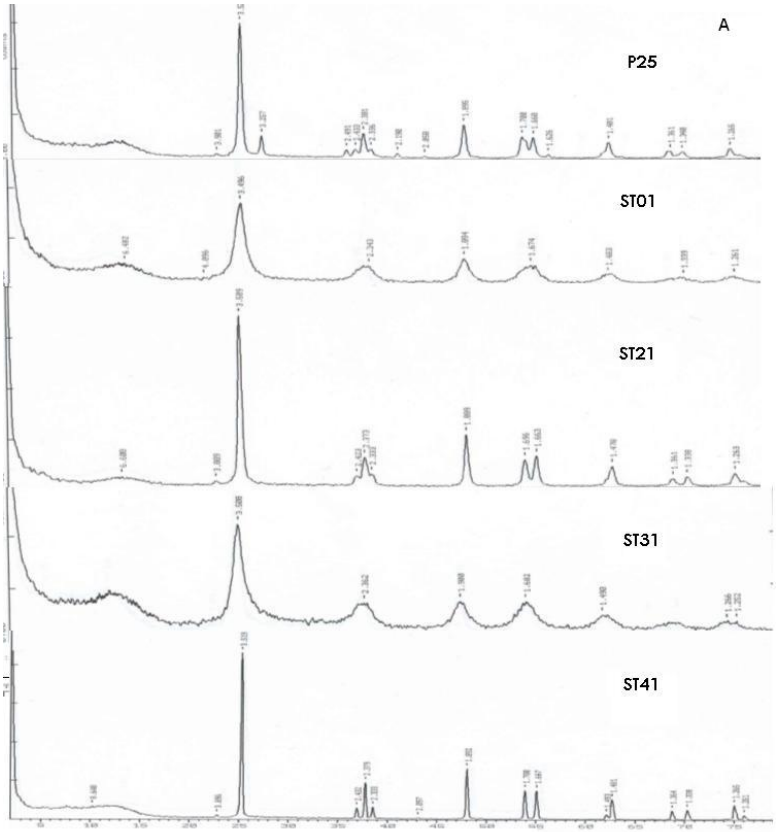

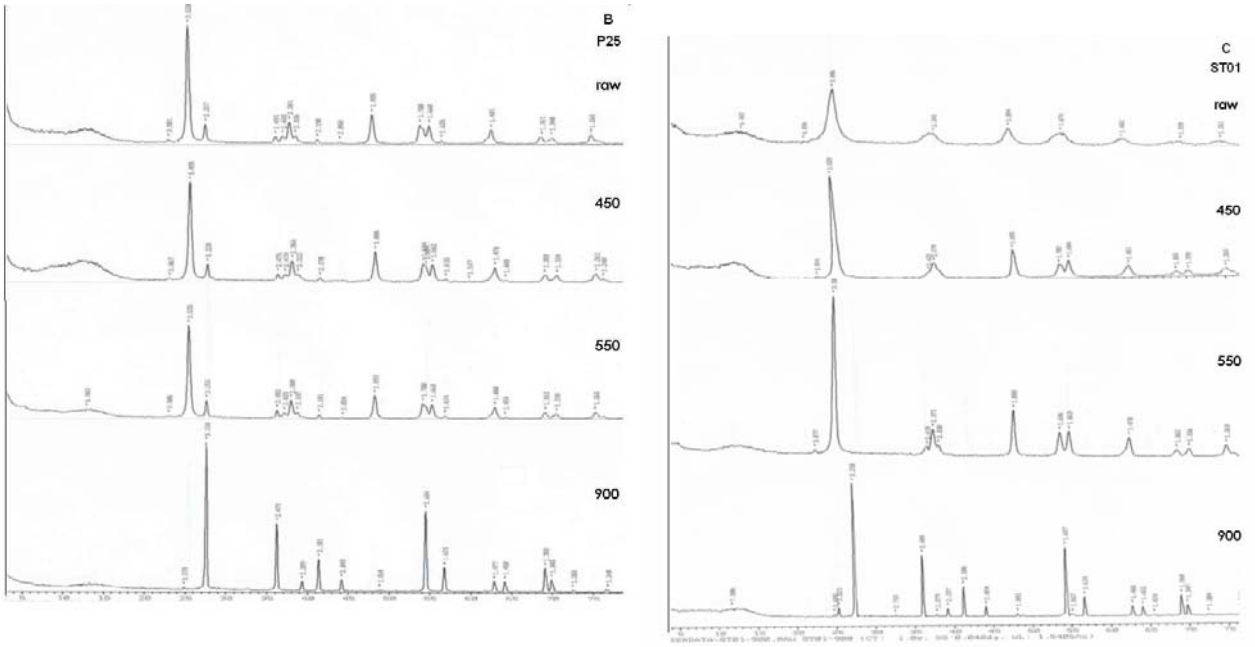

Fig. 24. The X-ray diffractograms of unheated TiO_2 samples (A), heated P25 (B), heated ST01 (C)

1.2 SEM

The SEM images of TiO_2 samples were shown in figure 25. We see that in ST01, ST21, ST31, the TiO_2 particles are stuck together to form the large cluster, but not in P25. All of TiO_2 particles are in nanometer size. Figure b showed the SEM image of ST01 heated at 900^oC, the particles was sintered into very large particles (hundreds of nanometer). This caused in decreasing the surface area, therefore lowered the dye adsorption capacity of TiO_2

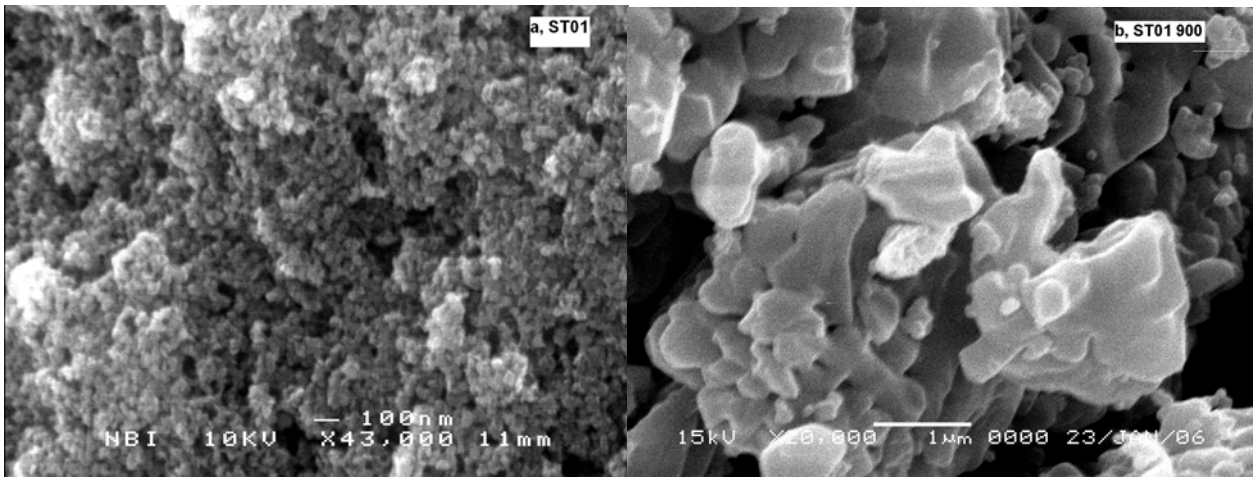

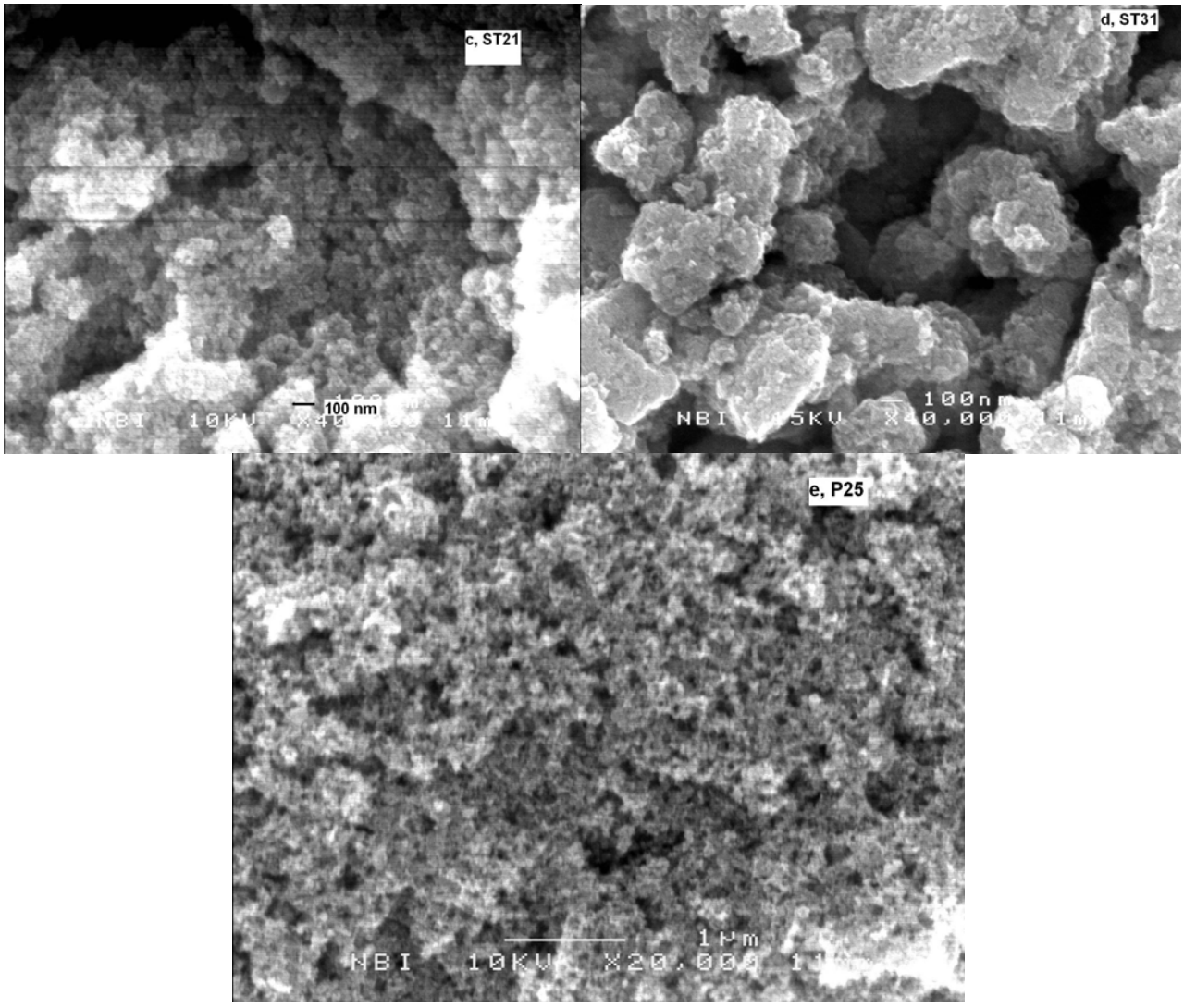

Fig. 25. The SEM of TiO_2 samples

The table 2 shows the characteristics of 5 types of TiO_2 [37].

Table 2: Characteristics of TiO_2 samples

Sample	**% wt.TiO_2**	**Surface area (m^2/g)**	**Size (nm)**	**Anatase/rutile**
P25	99.5	50	21	80/20
ST01	93.9	314	7	100/0
ST21	98.2	68	20	100/0
ST31	79.5	257	7	100/0
ST41	99.4	10	200	100/0

2. Degradation rate

2.1 Identification of dye degradation products

The typical HPLC-UV-MS chromatogram of the dye degradation products on ST01 with 600,000 counting of laser light was shown in figure 26:

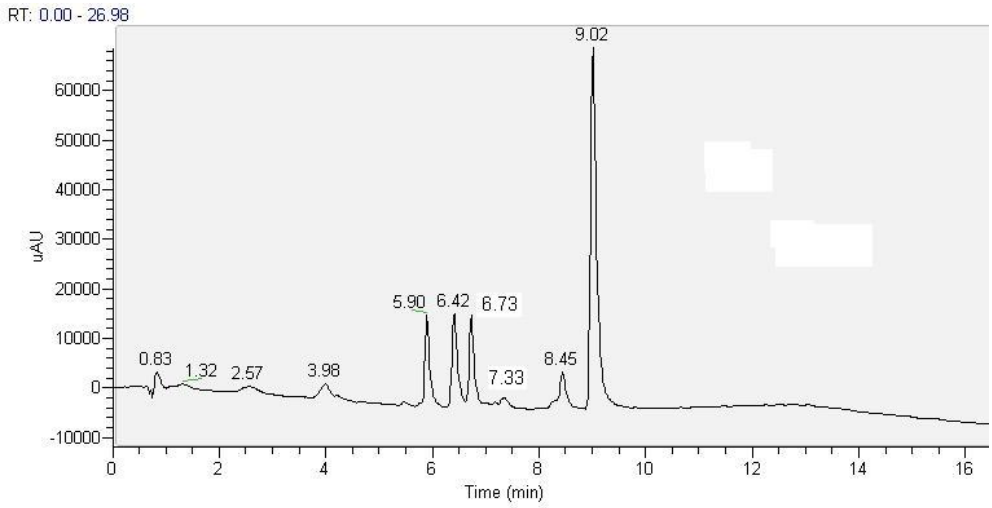

Fig. 26. The typical chromatogram of the dye degradation products

The m/z value and maximum absorption wavelength of the peaks was presented in the table 3. From the λmax and m/z values, we can identify the structures of degradation products [31, 40].

Table 3: Identification of the dye degradation products

Peak retention time (min)	Maximum absorption wavelength (nm)	m/z value	Structure
1.32	485	**632**; 646	$RuL_2(NC)(H_2O)^+$
2.57	493	**656**; 633	$RuL_2(NC)(ACN)^+$
3.98	486	**642**; 634	$RuL_2(NC)_2$
5.90	523	688; 648	$RuL_2(NCS)(H_2O)^+$
6.42	504	**674**; 694	$RuL_2(NCS)(NC)$
6.73	493	**688**; 674; 647	$RuL_2(NCS)(ACN)^+$
7.33	510	648	$RuL_2(NCS)(H)$
8.45	527	**706**; 648	$RuL_2(NCS)(SCN)$
9.02	533	**706**; 648; 723; 745	$RuL_2(NCS)_2$

In most of our photolysis experiments, the counting number was small, therefore, 4 main products were observed: $RuL_2(NCS)(NC)$, $RuL_2(NCS)(ACN)^+$, $RuL_2(NCS)(H_2O)^+$ and sometimes $RuL_2(NC)_2$. The MS spectrograms of the main degradation products were shown in fig 27.

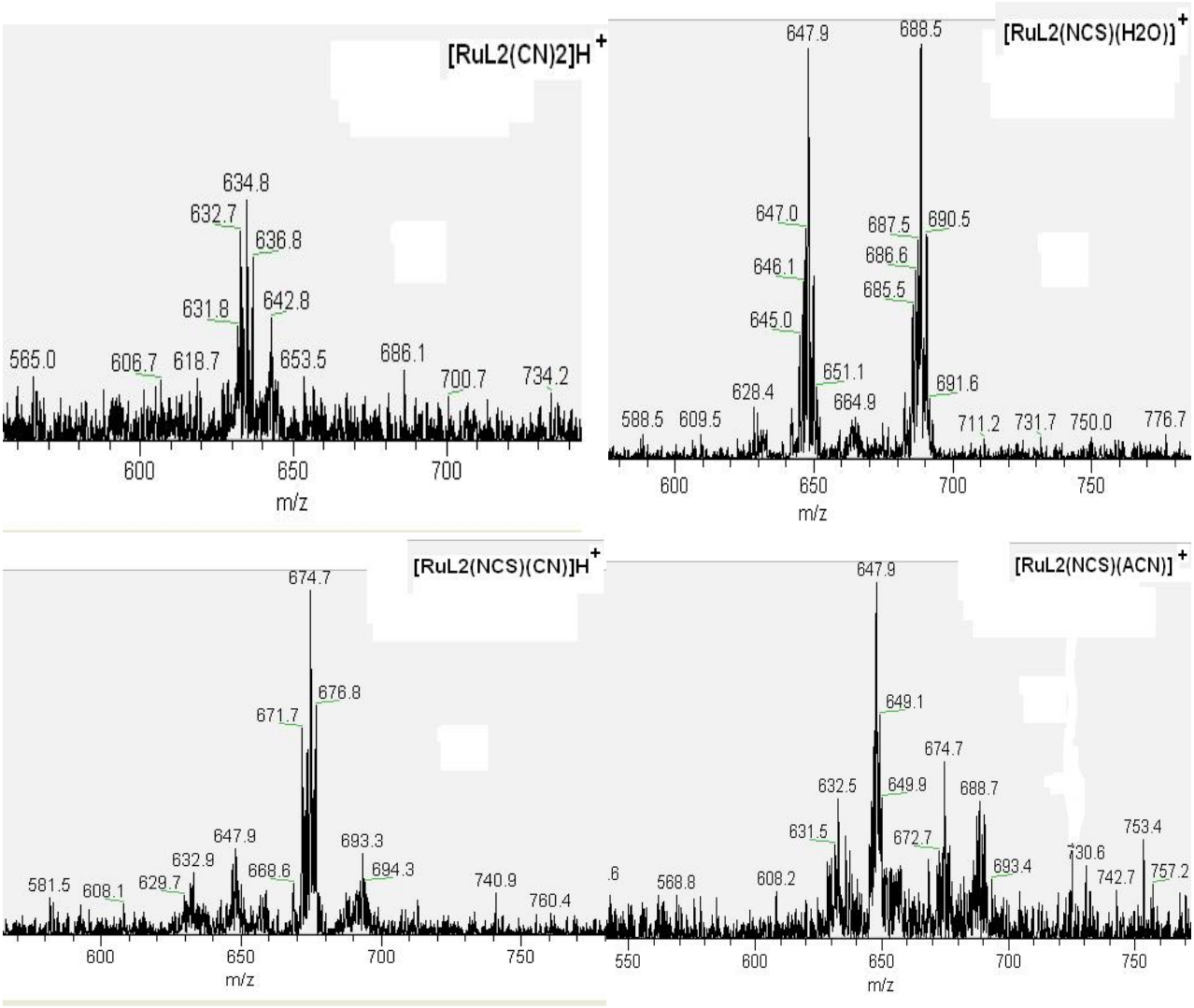

Fig. 27. The MS spectrograms of the main degradation products

In the beginning, we run HPLC-UV-MS sequences at capillary temperature 350 ^{o}C and we cannot see the m/z values of molecular ions. Then we lowered the capillary temperature to 200 ^{o}C, and we can observe all of molecular ions (figure 28)

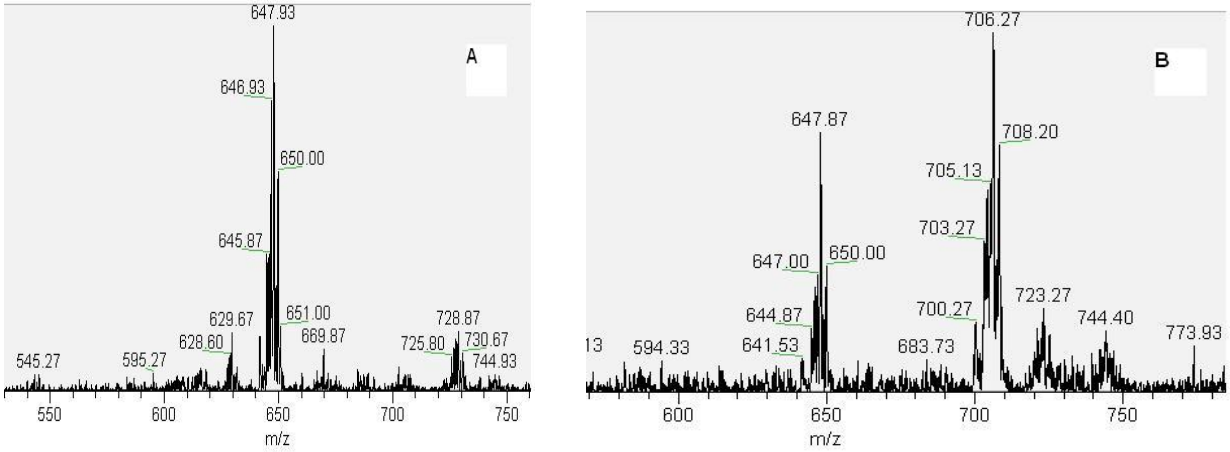

Fig. 28. Effect of capillary temperature on molecular ion peaks. (A) at 350^{o}C, (B) at 250^{o}C.

In figure a, the samples were run at capillary temperature 350 ^{o}C, the peak of N719 molecular ion with m/z 706 did not appear, but it occurred when capillary temperature was lowered to 200 ^{o}C in figure b. The peak m/z = 648 is $[RuL_2(NCS)(CN)H]^+$. Later approach helps us to identify of structures of degradation products.

2.2 Dark reaction

The dependence of time on degradation of N719 bound to TiO_2 particles in acetonitrile was shown on figure 29. It appeared that the degradation percent increased on time. It was difficult for us to determine what the degradation products increased because the amount of degradation products was small. The total degradation percent was not more than 5%. The degradation products increased slightly due to the slow exchange of NCS ligand with ACN that we have observed on the solution of N719 in acetonitrile (figure 30). After a long time, the solvent exchange product was formed on the solution of N719 in acetonitrile. The peak at 6.27 min in chromatogram was identified as $[RuL_2(NCS)(ACN)]^+$, m/z = 688.

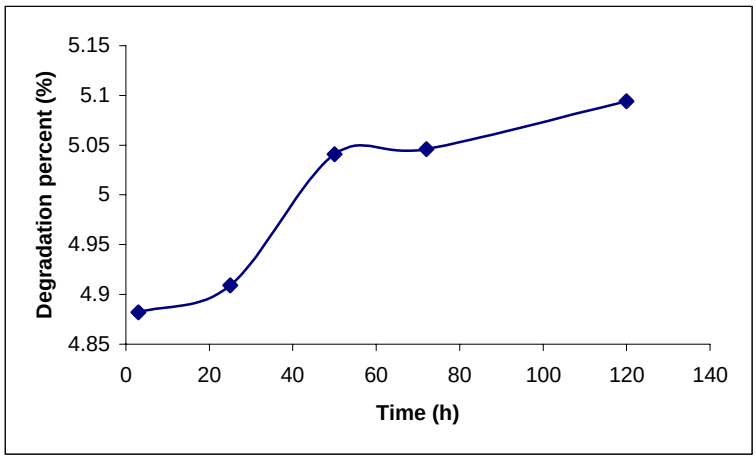

Fig. 29. Dependence of degradation on time

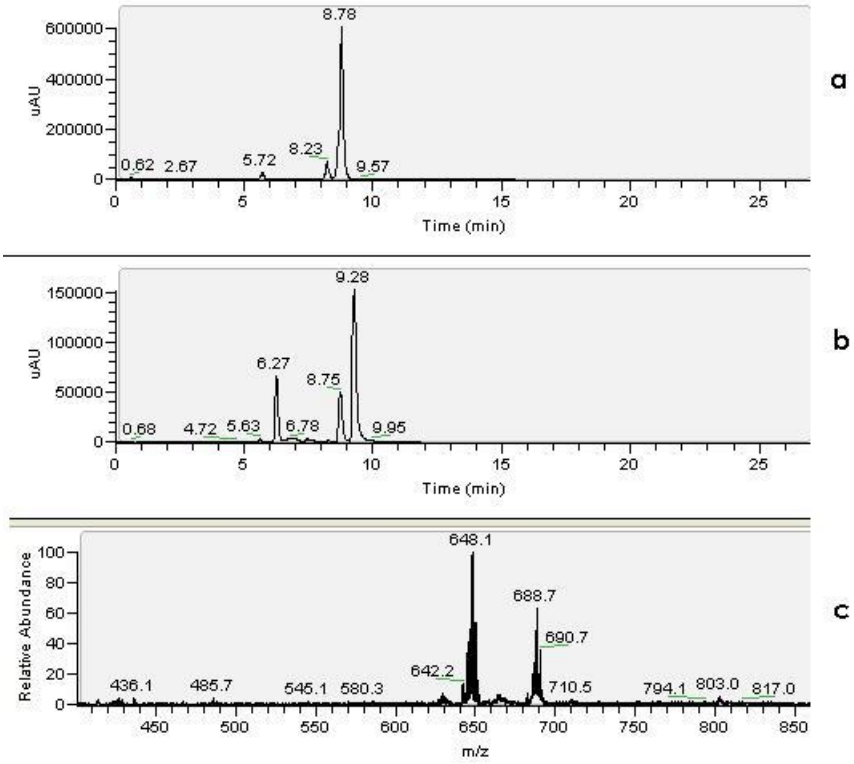

Figure 30. a, Chromatogram of N719 in ACN; b, Chromatogram of N719 in ACN after a long time; c, Mass spectrum of the peak at 6.27 min (in b).

The degradation without laser light photolysis was shown in table 4:

Table 4: Degradation percentage in case without photolysis.

Sample	% degradation products
P25	6.80
ST01	7.25
ST21	7.20
ST31	7.02
P25-ST21	6.22

Without the photolysis with the laser light, we found that N719 bound to the TiO_2 particles was degradation (fig. 31). The degradation products consist of three main products just as those in photolysis experiments. We did not see the product $[RuL_2(CN)_2]$. It can be concluded that the dye bound to TiO_2 can be degraded under the room condition. The degradation percent is more or less 7%. This numbers may be higher than the number in the time-dependent experiments because they were experimented a long time after the time-dependent experiments.

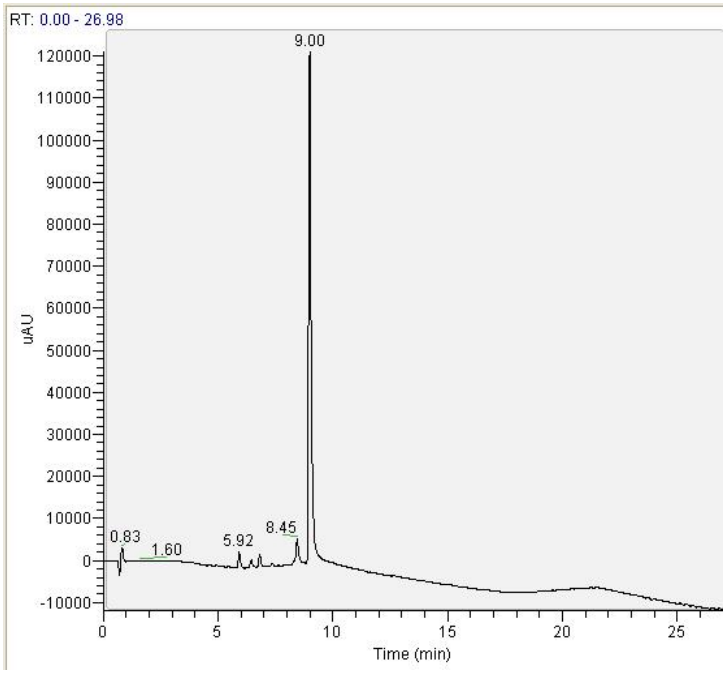

Figure 31. Chromatogram of degradation products of N719 bound to P25.

2.3 Photolysis

2.3.1 Effect of anatase/rutile ratio

From the characteristics of P25 and ST21, we see that they are nearly familiar in size, surface area and purity of TiO_2 amount, they only differ in. Therefore we based on two samples to investigate the effect of the anatase/rutile ratio on the degradation of N719 bound to TiO_2 particles. We knew from the X-ray diffractions that P25 consists of approximately 20% of rutile and 80% of anatase, ST21 is pure anatase. We also studied the N719 degradation on mixture of 50% P25 and 50% ST21, therefore we knew the N719 degradation on mixture consisting of 10% rutile and 90% anatase. The plot of mole of degradation products vs. mole of photon was shown in figure 32:

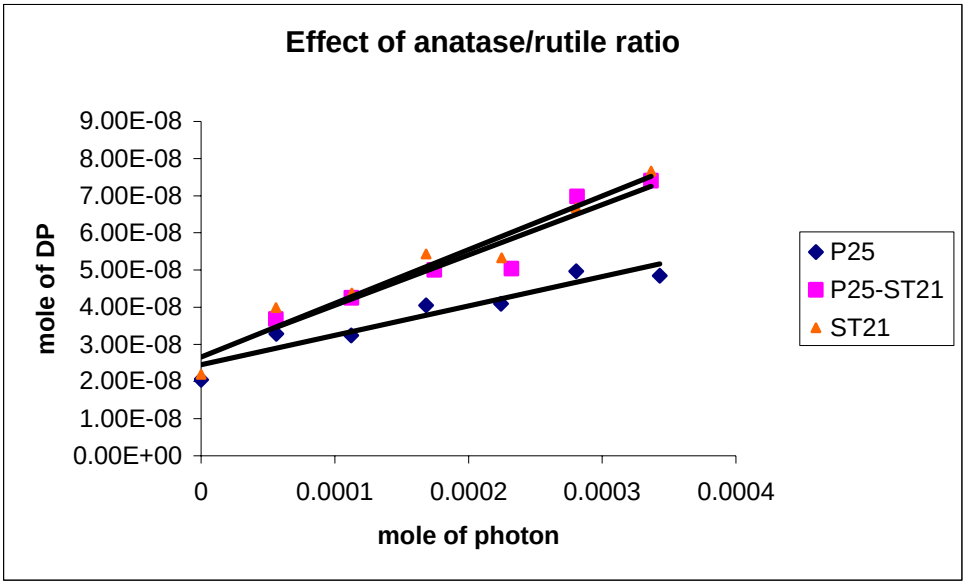

Fig. 32. Effect of anatase/rutile ratio on degradation.

The quantum yields of degradation processes were calculated from the plots (table 5). It is apparent that the quantum yield of degradation processes increases when the anatase amount of TiO_2 increased. This phenomenon is similar to which occurs in photocatalysis on TiO_2, the anatase type in most cases is more active than rutile type in degradation of organic pollutants [38].

Table 5: Quantum yields of degradation vs. anatase/rutile ratio

Samples	Anatase/rutile ratio	Quantum yield
P25	80/20	$7.90x10^{-5}$
P25-ST21	90/10	$1.35x10^{-4}$
ST21	100/0	$1.45x10^{-4}$

2.3.2 Effect of Oxygen

The effect of oxygen amount on degradation of N719 bound to P25 was shown in figure 33. The quantum yield of degradation processes is tabulated on table 6. We can see that the quantum yield increases when the oxygen amount increases from the absolutely free-oxygen to saturated-oxygen solutions . It is also suitable to the photocatalysis viewpoint. Shangjie Xu et al. observed the generation of active oxygen species ($O_2^{\cdot-}$, $^1O_2$, $^{\cdot}OOH$) in the system of TiO_2 sensitized by dye hypocrellin B when irradiated [39]. Maybe these active species have increased the degradation of N719. However, we have not investigated the mechanism of this process. Also, we did not see different kinds of degradation products in these processes.

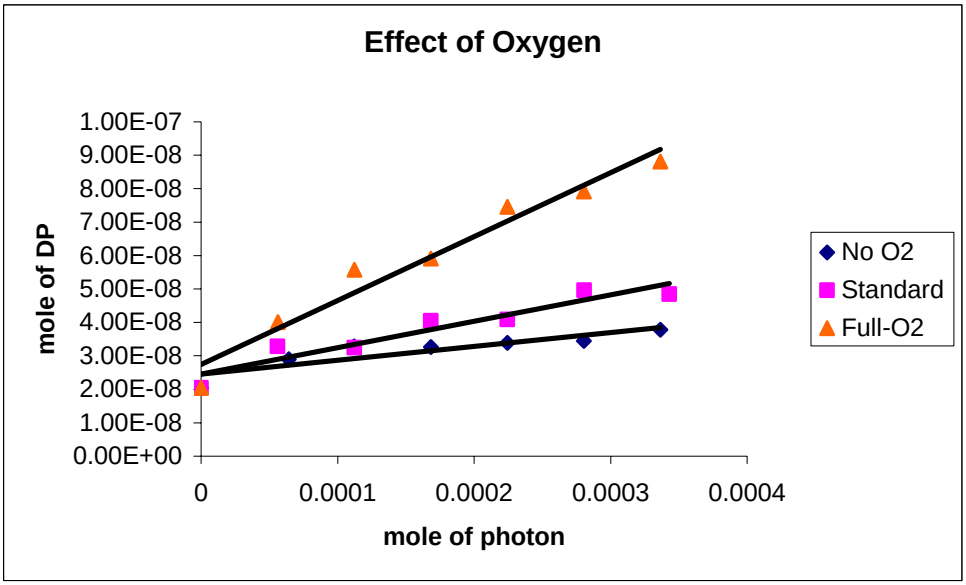

Fig. 33. Effect of oxygen on degradation

Table 6: Quantum yields of degradation vs. oxygen amount

Oxygen amount	Quantum yield
Free	$4.12x10^{-5}$
Standard	$7.90x10^{-5}$
Saturated	$1.91x10^{-4}$

2.3.3 Degradation of N719 on different TiO_2 types

Degradation of N719 was investigated on different kinds of TiO_2. The plots of amount of degradation products vs. amount of photon were presented in figure 34. The quantum yield of degradation processes was shown on the table 7. As we see, the photodegradation activities of ST01 and ST31 were larger than those of ST21 and P25. This is due to the larger surface area of the former ones. The surface areas of ST01 and ST31 are 314 and 257 m^2/g that was so ample when compared to those of ST21 and P25 (68 and 50 m^2/g respectively). The bigger surface area may contain the more numerous active sites causing the degradation of N719. The degradation activity of ST01 is so much than which of ST31. Besides the smaller surface area of ST31, its composition contains about 20% of ZnO instead of the pure anatase. The photodegradation activity of ZnO is always smaller than of TiO_2 anatase. The lower activity of P25 compared to ST21 is due to the smaller percentage of anatase.

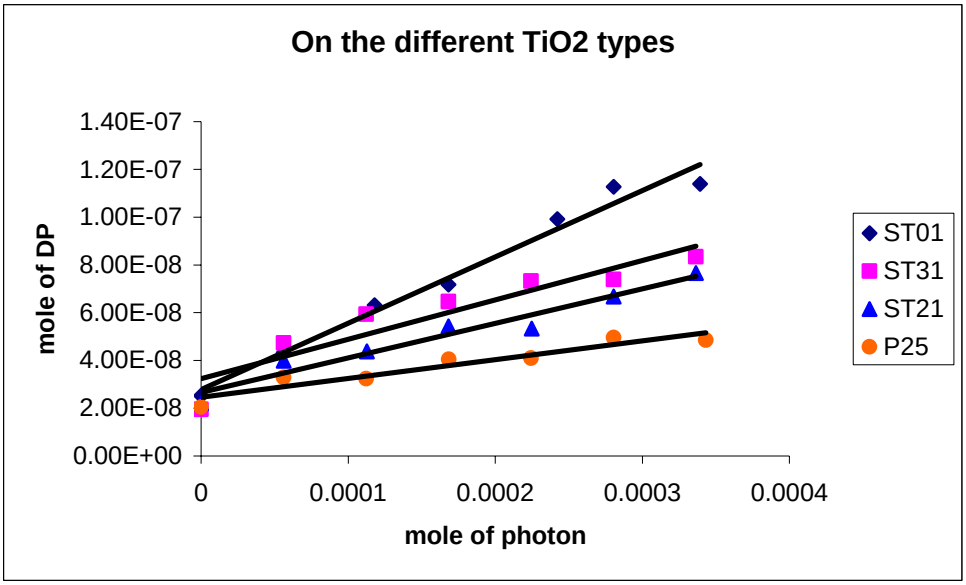

Fig. 34. Dye degradation on different TiO_2 types

Table 7: Quantum yields of degradation on different TiO_2 types

Samples	Quantum yield
P25	7.90×10^{-5}
ST21	1.45×10^{-4}
ST31	1.65×10^{-4}
ST01	2.78×10^{-4}

Conclusions

Degradation rate of N719 depends on structure of TiO_2. When the anatase/rutile ratio of TiO_2 increases, the degradation is higher. Also, the degradation rate increases if oxygen amount in the system increases. This lowered rapidly the life-time of the cell. Nevertheless, the chemistry of degradation products did neither depend on the anatase/rutile ratio of TiO_2 nor on the oxygen amount. The high surface areas of TiO_2 cause the high degradation of N719. The degradation product amount in room condition (normal light) is relatively small (from 5-7%).

We have successful prepared the solar cells. Due to the fact that time is limited, we have not measured the I-V curve, from which we can calculate the conversion efficiencies of the cells. However, we have tested the operation of the cells using Ohm-meter, and found that they worked well.

References

1. World energy report 2005, RWE Group, http://www.rwe.com.
2. A. Fujishima, K. Honda, *Nature* 1972, 238, 37.
3. A. Fujishima, X. Zhang, *C. R. Chimie* 2006, 9, 750.
4. F. Fujihara, T. Ohno, M. Matsumura, *J. Chem. Soc,. Faraday Trans.* 1998, 94, 3705.
5. T. Ohno, F. Tanigawa, K. Fujihara, S. Izumi, M. Matsumura, *J. Photochem. Photobio. A: Chemistry* 1998, 118, 41.
6. T. Ohno, F. Tanigawa, K. Fujihara, S. Izumi, M. Matsumura, *J. Photochem. Photobio. A: Chemistry* 1999, 127, 107.
7. S. U. M. Khan, M. Al-Shahry, W. B. Ingler Jr., *Science* 2002, 297, 2243.
8. L. Sun, L. Hammarstrom, B. Åkermark, S. Styring, *Chem. Soc. Rev*. 2001, 30, 36.
9. M. Yagi, M. Kaneko, *Chem. Rev.* 2001, 101, 21.
10. W. Ruttinger, G. C. Dismukes, *Chem. Rev*. 1997, 97, 1.
11. L. Hammarstrom, *Curr. Opin. Chem. Biol.* 2003, 7, 666.
12. K. Yamamoto, Y. Tawada, *Solar Energy* 2004, 77, 939.
13. M. A. Green, J. Zhao, A. Wang, S. R. Wenham, *Solar. Ener. Mater. Solar Cells* 2001, 65, 9.
14. A. Goetzberger, C. Hebling, H. Schock, *Mater. Sci. Eng. R Reports* 2003, 40, 1.
15. J. M. Nunzi, *C. R. Physique*, 2002, 3, 523.
16. H. Tshubomura, M. Matsumura, Y. Nomura, T. Amamiya, *Nature* 1976, 261, 402.
17. B. O'Regan, M. Gratzel, *Nature* 1991, 353, 737.
18. M. Cratzel, *Inorg. Chem*. 2005, 44, 6841.
19. M. K. Nazeeruddin, A. Kay, I. Rodicio, R. H. Baker, E. Muller, P. Liska, N. Vlachopoulos, M. Cratzel, *J. Am. Chem. Soc.* 1993, 115, 6282.
20. M. K. Nazeeruddin, S. M. Zakeeruddin, R. H. Baker, M. Jirousek, p. Liska, N. Vlachopoulos, V. Shklover, C. H. Fisher, M. Gratzel, *Inorg. Chem*. 1999, 38, 6298.
21. M. Nazeeruddin, C. Klein, P. Liska, M. Gratzel, *Coord. Chem. Rev.* 2005, 249, 1460.
22. P. Wang, C. Klein, P. R. H. Baker, S. M. Zakeeruddin, M. Gratzel, *J. Am. Chem. Soc.* 2005, 127, 808.

23. M. Nazeeruddin, M. Gratzel, *J. Am. Chem. Soc. 2001,* 123, 1613.
24. S. Pavasupree, S. Yoshikawam *J. Photochem. Photobiol. A* 2006, in press.
25. C. Lao, D. Zou, *Sol. Energy Mater. Sol Cells* 2005, 85, 457.
26. L. N. Wang, M. Muhammed, *J. Phys. Chem. B* 1997, 101, 2598.
27. A. Hagfeldt, M. Cratzel, *Chem. Rev*. 1995, 95, 49.
28. H. G. Agrell, J. Lindgren, A. Hagfeldt, *Solar Energy* 2003, 75, 169.
29. H. Greijer, J. Lindgren, A. Hagfeldt, *J. Phys. Chem. B*. 2001, 105, 6314.
30. F. Nour-Mohhamadi, D. S. Nguyen, G. Boschloo, A. Hagfeldt, T. Lund, *J. Phys. Chem. B* 2005, 109, 22413
31. F. Nour-Mohammadi, T. H. Nguyen, G. Boschloo, T. Lund, manuscript for publication.
32. Nguyen Doan Sau, Master Thesis, Roskilde University, 2004
33. Photochromic fulgides as chemical actinometers, School of Chemistry and Applied Chemistry,University of Wales College of Cardiff.
34. The use of Aberchrome 540 in chemical actinometry, School of Chemistry and Applied Chemistry, University of Wales College of Cardiff.
35. The preparation of the ASC/NSC sealed glass cells from the Hagfelts group, Royal Institute of Technology, Sweden, 2003..
36. V. Ramamurthy, Kirk S. Schanze, Semiconductor Photochemistry and Photophysics, Marcel Dekker, 2003, p. 142
37. Characteristics documents of TiO_2 from Ishihara Company, Japan.
38. M. Kaneko, I. Okura, Photocatalysis Science and Technology, Springer, 2002, p. 158.
39. S. Xu, J. Shen, S. Chen, M. Zhang, T. Shen, *J. Photochem. Photobio. B,* 2002, 67, 64
40. G. Hansen, B. Gervang, T. Lund, *Inorg. Chem.* 2003, 42, 5545.